COURSE 9

ATOMIC HYDROGEN AND LIQUID HELIUM SURFACES

J.T.M. WALRAVEN

Van der Waals–Zeeman Laboratorium, Universiteit van Amsterdam
Valckenierstraat 65/67,
1018 XE Amsterdam, The Netherlands

J. Dalibard, J.M. Raimond and J. Zinn-Justin, eds.
Les Houches. Session LIII. 1990
Systèmes Fondamentaux en Optique Quantique
/Fundamental Systems in Quantum Optics

Contents

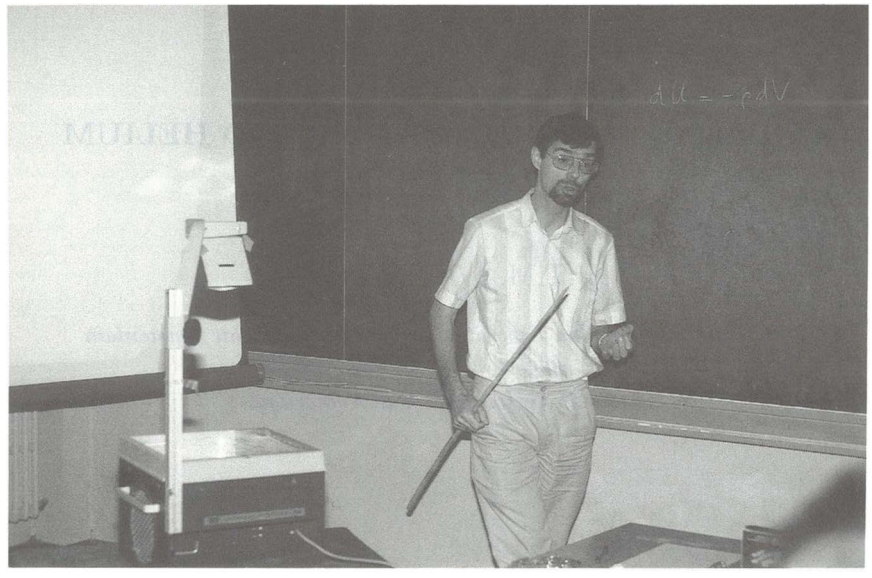
dU = -pdV

1. Introduction

Over the last decade there has been a wave of interest and important progress in spin-polarized hydrogen research. The motivation for studying this subject may be traced back to the unique properties of atomic hydrogen and deuterium as *the only* quantum gases. The light mass and the weak non-binding $b\text{-}^3\Sigma_u^+$ interaction between two spin-polarized hydrogen atoms lead to a positive internal energy and hence to a gaseous nature down to the absolute zero of temperature. The gas is interesting from widely different points of view. Apart from the purely scientific interest in its properties the cryogenic hydrogen maser is possibly technologically important. One may also single out the recombination reaction $2H+X \rightarrow H_2+X$ as one of the fundamental reactions of quantum chemistry or mention exotic collective phenomena such as nuclear spin waves. Others consider the relevance of H-research for the ongoing efforts to create and trap antihydrogen. A goal of central importance that probably drew most attention to the field has been the search for quantum degeneracy effects such as Bose Einstein condensation (BEC) in the bulk gas or the Kosterlitz Thouless transition (KTT) in H gas adsorbed on the surface of liquid helium.

Rather than touching upon many of these different subjects with the aim of giving an overview, in the written version of these lectures the subject is restricted to various aspects of the interplay of hydrogen with the surface of liquid helium. Surface related phenomena are of vital importance to all experimental activity in the field and important progress has been reported over the last few years. Covering new aspects, the present text is supplementary to comprehensive reviews by Tom Greytak and Daniel Kleppner [1] and that of Ike Silvera and myself [2]. Other reviews having a similar supplementary nature were written by Walter Hardy and collaborators on zero-field magnetic resonance work [3, 4] and on spin-waves by Jack Freed [5] and David Lee [6].

The paper is organized as follows. After an introduction covering fundamental properties and nomenclature in section (2), the main subject is

divided in two parts. The first part, section (3) deals with the static properties of the adsorbed state of atomic hydrogen on liquid helium. This includes both single-atom and gas-phase properties. The other main part, section (4) deals with the collisional properties of hydrogen atoms colliding with helium surfaces. The paper is concluded with a discussion of experimental results and a look at the future.

2. Fundamentals

2.1. Atomic constants and hyperfine structure

Hydrogen and its isotopes (H, D and T) form one-electron atoms with a $^2S_{1/2}$ ground state. The proton and triton have spin $i = \frac{1}{2}$. The deuteron has spin $i = 1$. The corresponding nuclear magnetic moments follow from $\mu_n = g_n \mu_N \boldsymbol{i}$. The magnetic moment of the electron is given by $\mu_e = -g_e \mu_B \boldsymbol{s}$. Here we use the notation μ_B and μ_N for the Bohr and nuclear magnetons, respectively, and g_e and g_n for the associated g factors. In terms of these constants the gyromagnetic ratios are defined by $\gamma_e = g_e \mu_B / \hbar$ and $\gamma_n = g_n \mu_N / \hbar$, where $2\pi\hbar$ is the Planck constant. The recommended values for the free-particle atomic constants of electron, proton and deuteron are in respective order [7]

$$\gamma_e = 1.760\,859\,23(53) \times 10^{11}\ \mathrm{s^{-1}T^{-1}}$$
$$\gamma_p = 2.675\,221\,28(81) \times 10^{8}\ \mathrm{s^{-1}T^{-1}}$$
$$\gamma_d = 4.106\,628(2) \times 10^{7}\ \mathrm{s^{-1}T^{-1}}\ ,$$

and,

$$g_e/2 = \mu_e/\mu_B = 1.001\,159\,625\,193(10)\ ,$$
$$g_p/2 = \mu_p/\mu_N = 2.792\,847\,386(63)\ ,$$
$$g_d = \mu_d/\mu_N = 0.857\,438\,230(24)$$

with $\hbar = 1.054\,572\,66(63) \times 10^{-34}$ J s, $\mu_B = 9.274\,015\,4(31) \times 10^{-24}$ J T^{-1} and $\mu_N = 5.050\,786\,6(17) \times 10^{-27}$ J T^{-1}.

To introduce some nomenclature relevant to this paper the hyperfine structure of the ground-state manifold is discussed in some detail for the isotope H. The Hamiltonian for this problem involves the Zeeman and the

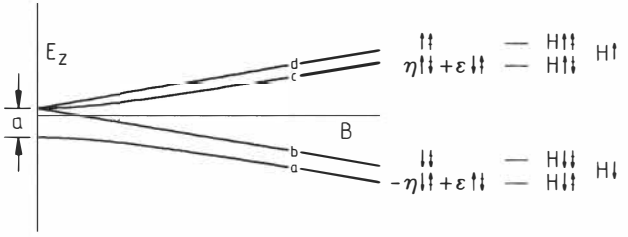

Fig. 1. The hyperfine structure of the 1S manifold of the hydrogen atom. Here $\eta = \cos\theta$ and $\varepsilon = \sin\theta$. The other symbols are defined in the text.

Fermi contact hyperfine interactions:

$$H = -(-g_e\mu_B \boldsymbol{s} + g_n\mu_N \boldsymbol{i})\cdot \boldsymbol{B} + a\boldsymbol{i}\cdot\boldsymbol{s} \ . \tag{2.1}$$

Here a is the hyperfine constant and $\boldsymbol{B}$ the applied magnetic field. Diagonalization for $s = \frac{1}{2}$ and $i = \frac{1}{2}$ leads to the well known Breit–Rabi [8] energy level diagram shown in fig. 1 with a zero-field hyperfine splitting

$$\nu_0 \equiv \frac{a}{h} = 1\,420.405\,751\,733(1) \text{ MHz} \ .$$

In zero field $\boldsymbol{f} = \boldsymbol{i} + \boldsymbol{s}$ and m_f are good quantum numbers, whereas in high fields ($B \gg a/\mu_e \simeq 507$ Gauss) this holds for m_s, m_i and m_f. By convention, in spin-polarized hydrogen research the ground state hyperfine levels are labeled a, b, c and d in order of increasing energy in small magnetic field. The b and d states are pure spin states, the a and c states are hyperfine mixed linear combinations of the high field basis states $|m_s, m_i\rangle$:

$$\begin{aligned} |\mathrm{d}\rangle &= |\uparrow\uparrow\rangle, \\ |\mathrm{c}\rangle &= \cos\theta|\uparrow\downarrow\rangle + \sin\theta|\downarrow\uparrow\rangle, \\ |\mathrm{b}\rangle &= |\downarrow\downarrow\rangle, \\ |\mathrm{a}\rangle &= \sin\theta|\uparrow\downarrow\rangle - \cos\theta|\downarrow\uparrow\rangle, \end{aligned} \tag{2.2}$$

where

$$\tan 2\theta \equiv a/[\hbar(\gamma_e + \gamma_p)B] \ . \tag{2.3}$$

The simple arrows ↑ and ↓ refer to the magnetic quantum number of the electron spins and crossed arrows ↑ and ↓ to that of the proton spins. The gas phase is characterized by the spin-polarization of the constituent atoms. Unpolarized gas is referred to as H, up or down electron-spin-polarized gases as H↑ and H↓ respectively. Further one distinguishes the doubly (both electron and proton spin) polarized gases, consisting predominantly of b-state (H↓↓) or d-state (H↑↑) atoms. Sometimes it is convenient to label the atoms by the direction of the force caused by a magnetic field gradient. For this purpose the terminology high-field-seekers (for H↓) and low-field-seekers (for H↑) is used. An analogous notation and terminology is used for deuterium and tritium.

2.2. Interaction potentials

The interaction between two H-atoms depends on the spin states of the atoms. Thus, the four 1S hyperfine states give rise to 16 potential curves, 11 of which are distinct in zero field (for D–D 22 out of 36). However, for most practical purposes the hyperfine interaction may be neglected and a description in terms of the $X\text{-}^1\Sigma_g^+$ and $b\text{-}^3\Sigma_u^+$ potentials is adequate. These potentials are calculated to high precision by Kolos and Wolniewicz [9–12]. Both singlet and triplet potentials are shown in fig. 2. Spin-polarized hydrogen atoms interact via the triplet potential. This interaction has a very weak attractive minimum, only 6.5 K deep. This is at the origin of the low-temperature stability of the gas phase. The triplet potential does not support a many-body bound state even at $T = 0$ K. To assure the dominance of the triplet potential electron-spin-flips have to be avoided in experiments. A convenient fitting function for the triplet potential has been given by Silvera [39]:

$$V_t(r) = \exp(0.096\,78 - 1.101\,73r - 0.039\,45r^2) - F_c(r)(6.5r^{-6} + 124r^{-8} + 3285r^{-10})\,. \tag{2.4}$$

The cutoff function is defined by

$$F_c(r) = \exp - \left(\frac{10.04}{r} - 1\right)^2 \qquad r < 1.28r_{\min}, \tag{2.5}$$

$$= 1, \qquad r > 1.28r_{\min}, \tag{2.6}$$

where $r_{\min} = 4.16$ Å is the minimum in the $V_t(r)$ curve. The hard core of the triplet is defined by the zero crossing $r_0 = 3.68$ Å. The exchange energy

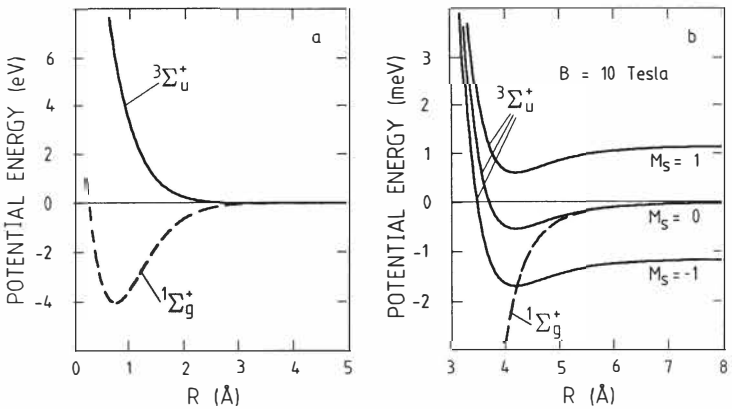

Fig. 2. The singlet and triplet interatomic potentials as calculated by Kolos and Wolniewicz. (b) shows the lifting of electron-spin degeneracy by a magnetic field on a magnified vertical scale with respect to (a).

is defined by $J(r) \equiv V_t(r) - V_s(r)$. For internuclear distances in the range $a_0 < r < 12\,a_0$ [39]

$$J(r) = \exp(-0.288 - 0.275r - 0.176r^2 + 0.0068r^3). \tag{2.7}$$

In eqs. (2.4) and (2.7) atomic units are used (1 hartree = 219 474.6 cm^{-1}, $a_0 = 0.529\,177$ Å = 1 bohr).

3. Hydrogen adsorbed on the surface of liquid helium

Liquid helium surfaces play an important role in studies of gaseous atomic hydrogen at low temperature. This arises because in experiments the sample cells are coated with liquid helium films to avoid massive surface adsorption of the H atoms followed by recombination to the molecular state H_2. Helium films are used for this purpose as they are chemically inert and provide the smallest conceivable atom–surface interaction to the H atoms. The presence of helium does not seriously affect the vacuum regime in the experiments, as at $T = 300$ mK the density of the saturated vapor of ^{4}He is only $n = 1 \times 10^{10}$ cm^{-3}, which represents a high vacuum. Moreover this density falls exponentially with decreasing temperature in accordance to the latent heat of vaporization, $L_4 = 7.16$ K for ^{4}He at $T = 0$ K. Hence,

the vapor pressure may be reduced to almost any desired level by reducing the temperature. It is of course extremely important to understand how the presence of the helium film affects experiments with H. First of all one would like to know whether H dissolves in liquid helium, or if it is bound to the helium surface.

From an experimental point of view it is well-established that H does not dissolve in liquid helium but may become adsorbed onto the gas–liquid interface [1, 2]. Much effort has been invested from the theoretical side to understand these findings in terms of a microscopic theory. For this purpose the theory of binary boson mixtures was applied and further developed for the hydrogen impurities by Miller [57, 15], Guyer and Miller [16], Ristig et al. [17] and Kürten and Ristig [18]. For our discussion, the quantities of interest are the energy required to dissolve an impurity atom in liquid ^{4}He, ε_s, and the effective mass m^* of the impurity.

We first address ε_s, the effective mass will be discussed in section 3.1 To obtain values for ε_s we use the results of Kürten and Ristig who calculated the chemical potential μ for *replacing* one ^{4}He atom from the liquid by one H, D or T atom [18]. Subtracting from μ the energy L_4 to obtain ε_s, one finds $\varepsilon_s = 36$, 14 and 6 K, respectively, for the liquid at the experimental zero-pressure density $\rho = 0.021$ Å^{-3}. These values where used by Reynolds et al. [25] to estimate the lifetime of samples of H, D and T due to solution into ^{4}He, followed by adsorption on the film substrate with subsequent recombination. Reynolds et al. calculate for typical experimental conditions and a temperature $T = 1$ K lifetimes of 9400 year, 120 s and 50 ms for H, D and T, respectively. The experimentally observed value for D is 6 s at $T = 1.1$ K [25]. Also unsuccessful attempts by Tjukanov et al. [19] to observe T around $T = 1$ K may well be explained in terms of loss of atoms due to penetration in the helium film. Decay of H samples through this mechanism is clearly too slow for experimental observation.

Although H will adsorb to helium surfaces its adsorption energy ε_a, defined as the energy required to remove an atom from the surface to infinity, is very small. For H on ^{4}He $\varepsilon_a/k_B = 1.00(5)$ K [4]. As we shall discuss in section 3.6, in the low-density, high-temperature limit the adsorption isotherm, relating the density of the adsorbed gas n_a to the bulk density n_g is given by

$$n_a = n_g \Lambda \exp(\varepsilon_a/k_B T) \ , \tag{3.1}$$

where $\Lambda = (2\pi\hbar^2/mk_B T)^{1/2}$ is the thermal de Broglie wavelength of particles with mass m. The generally accepted picture is that the atoms are highly mobile in the adsorbed state and are eventually desorbed after a

residency time τ_a that ranges from 1×10^{-8} s at 400 mK to 3×10^{-4} s at 100 mK. An expression for the residency time τ_a

$$\tau_a = \frac{2\pi\hbar}{s k_B T} \exp(\varepsilon_a / k_B T) \tag{3.2}$$

is obtained by balancing the flux of adsorbing atoms $\Phi_s = s\Phi$ against the flux of desorbing atoms $\Phi_d = n_a A \tau_a^{-1}$ for thermal equilibrium conditions. Here s is the adsorption probability (sticking coefficient), $\Phi = \frac{1}{4} n_g \bar{v} A$ is the total incident flux of atoms with A the surface area and $\bar{v} = (8k_B T/\pi m)^{1/2}$ is the average atomic speed. For $T \gtrsim 0.3$ K and densities $n_g \lesssim 10^{16}$ cm^{-3} the surface coverage will be very low and consequently loss of sample due to molecule formation on the surfaces will be effectively suppressed [2]. The limit of high coverage has some very interesting features which recently attracted new attention, but a discussion of this regime will be postponed to section 3.6

The properties of liquid helium surfaces are very interesting in their own right and have been the subject of numerous experimental and theoretical studies. The free surface has been reviewed by Edwards and Saam [37] and by Edwards [21]. A recent compilation of articles on bulk and surface excitation of the quantum fluids has been made by Wyatt and Lauter [22]. For many practical purposes the liquid and its surface may be considered to be in their ground state, since for temperatures $T < 0.5$ K the superfluid fraction of the liquid approaches unity. For temperatures of experimental interest, $T \lesssim 1$ K, the thermal wavelength of H atoms is rather large ($\Lambda T^{1/2} \simeq 17.5$ ÅK$^{1/2}$), much larger than the average nearest neighbor distance between helium atoms in the liquid (3.5 Å). In this sense the surface is flat. There is no evidence for any appreciable polarization of the surface due to the adsorbed atoms. However, the surface is not static. The interface fluctuates due to the presence of elementary excitations, in particular ripplons (quantized capillary waves).

3.1. Hydrogen as a quasi-particle in liquid helium

It is desirable to have a physical picture of the behavior of hydrogen-like impurities in liquid helium. This may be obtained in an elementary form using the volume coefficient α, which relates the mass density of a dilute mixture to the density of the pure liquid at the same pressure and which is a measure for the size of the dressed impurity. This coefficient is calculated by Kürten and Ristig for H and T in liquid ^{4}He [18]. First we estimate the effective mass of the impurities. In order to move through the liquid,

the atoms have to displace the superfluid. As the atom–liquid interaction is repulsive and the superfluid behaves as a ideal irrotational fluid [23], an elementary estimate for the effective mass can be made by treating the impurity atoms as simple classical spheres [24]. A sphere of mass m moving through an irrotational fluid of mass density ρ experiences no frictional force, as is well known from classical hydrodynamics, but its apparent mass $m_{\rm cl}$ is enhanced according to

$$m_{\rm cl} = m + \tfrac{1}{2}\rho\nu \ , \tag{3.3}$$

where ν is the volume of the fluid displaced by the sphere. This model may be applied to impurities in ^{4}He by writing $\rho = m_4 n_4$, where m_4 is the mass and n_4 the number density of ^{4}He. With the relation

$$n_4\nu = 1 + \alpha \tag{3.4}$$

and identifying $m_{\rm cl}$ with the effective mass of the impurity, eq. (3.3) may be rewritten as

$$m^*/m_4 \simeq [m/m_4 + \tfrac{1}{2}(1+\alpha)] \ . \tag{3.5}$$

This procedure yields $m^*/m_4 = 1.4$ for ^{3}He impurities ($\alpha \simeq 0.31$), which is not at all bad in view of the experimental value $m^*/m_4 = 1.78$ [24]. Using $\alpha \simeq 12$ as calculated by Kürten and Ristig [18], one finds $m^*/m_4 = 6.75$ for H. Similarly, $\alpha \simeq 4.5$ yields $m^*/m_4 = 3.5$ for T. Unfortunately, the deuterium case, for which some experimental information is available [25], is not discussed in the literature, but one may argue that the H and T values clearly represent an upper and lower limit for this case. The large values for the volume coefficient and effective mass of the H-impurity suggest the picture that the zero-point motion of the atoms induces a bubble-like cavity in the liquid in which the repulsive forces between atoms and liquid are balanced by the surface tension.

Using eq. (3.4) one may estimate the radius of the effective volume for an H quasi-particle to be $r_{\rm e} = 5.2$ Å. For T one finds $r_{\rm e} = 3.9$ Å. ^{3}He-like quasi-particles are known to have free-particle-like dispersion curves [26]. With the effective masses estimated above one easily shows that around $T = 1$ K, atoms with sufficient energy to penetrate the liquid may create quasi-particles with typical velocities up to $v = (8k_{\rm B}T/\pi m^*)^{1/2} \simeq 30$–$40$ ms^{-1}. The critical velocity $v_{\rm c}$ for creation of a single roton by the impurity is $v_{\rm c} = \Delta/p_0 + p_0/2m^* \simeq 80$–$100$ ms^{-1} [27]. Here $\Delta/p_0 = 62.5$ ms^{-1} is the Landau critical velocity, $\Delta/k_{\rm B} = 8.65$ K being the roton gap and $p_0/\hbar =$

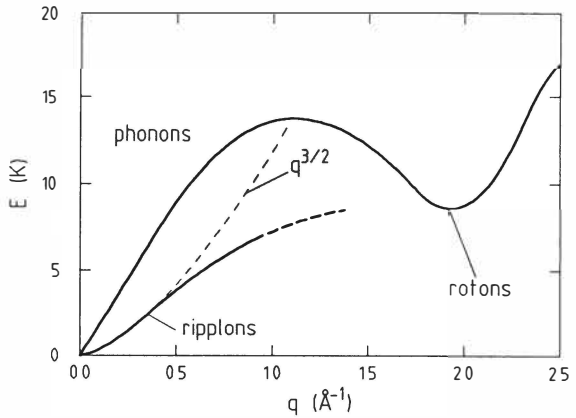

Fig. 3. Dispersion curves for elementary excitations in liquid helium and on the liquid–vapor interface. Note the deviation from the $q^{3/2}$ behavior for large q.

1.91 Å^{-1} the wavevector at the roton minimum. From these estimates one may infer that the H quasi-particles should behave much alike ^{3}He in liquid ^{4}He. Dispersion curves of excitations in layers of liquid helium are shown in fig. 3. We return to these excitations and their relevance for atomic hydrogen research in subsequent sections.

One may not a priori exclude the possibility that a velocity of 30 ms^{-1} is sufficient to create a vortex ring of radius $r_v = 5.2$ Å around the H quasi-particle when an H atom penetrates the fluid. Vortex ring excitation is well-known for ions in liquid ^{4}He. However these ionic quasi-particles are much larger, having effective masses exceeding $100m_4$ [28]. A vortex ring may be formed if the speed of the quasi-particle exceeds the translational velocity ν of a vortex with the same radius as the quasi-particle. For a classical vortex ring of radius r_v and core radius ξ the translational velocity is given by [28]

$$\nu = \left(\frac{\kappa}{4\pi r_v}\right)\left[\ln\left(\frac{8r_o}{\xi}\right) - \frac{1}{4}\right]. \tag{3.6}$$

Here $\kappa = 2\pi\hbar/m_4$ is the quantum of vorticity. Substituting figures one arrives at $\nu = 47$ ms^{-1}, which makes vortex excitation unlikely around $T = 1$ K for H quasi-particles, although it cannot be excluded in view of the rough model used here. As D and T quasi-particles are smaller, vortex

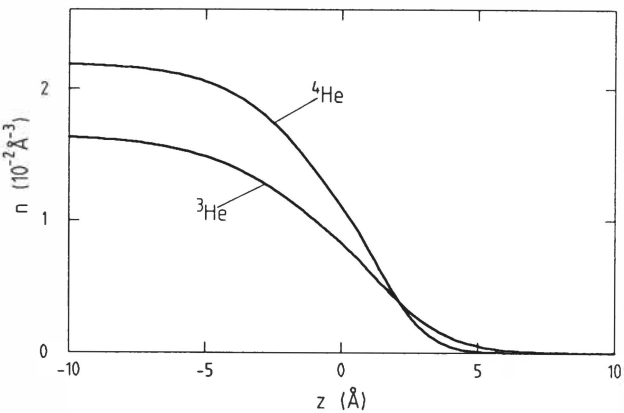

Fig. 4. Density profile of the free surface of liquid ^{4}He and ^{3}He according to Stringari and Treiner. For ^{4}He the density drops from 90% to 10% of the bulk value over a distance of 7 Å. For ^{3}He this distance is 8.3 Å.

creation should be less probable in these cases. Vortex creation in ^{4}He is recently reviewed by McClintock and Bowley [29].

3.2. Properties of single adsorbed atoms

Knowledge of the interaction between hydrogen atoms and the surface of liquid helium is of great importance to understand the surface adsorbed state of H gas as well as surface related phenomena like the kinetics of adsorption or surface catalyzed recombination. Some impression of the surface of liquid helium may be obtained from fig. 4 in which we reproduce the surface density profiles of ^{4}He and ^{3}He as calculated and reviewed by Stringari and Treiner [30]. The density profile is an important but by no means the only quantity to characterize the liquid surface. For a proper description one has to take into account the structure and dynamics of the liquid and correlations in motion between the hydrogen and the helium atoms.

If the atom is at large distance from the surface the problem is relatively simple. One may write a surface adsorption potential, simply by adding the long range contributions of the interactions between the H atom and the helium atoms constituting the liquid. For a pair interaction with Lennard-Jones r^{-6} long range behavior this results in a z^{-3} dependence if z is the distance above the surface. This approach was taken by Stwalley to make a

model with nice scaling properties of the adsorption energy for the hydrogen isotopes on liquid ^{3}He and ^{4}He [31]. The repulsive forces are accounted for in his model simply by putting a hard wall at $z = z_0$, where z_0 is chosen so as to fit the experimental binding energy of one of the isotopes. The difference in binding between H on ^{3}He and H on ^{4}He arises solely from the difference in density of the liquids.

To obtain a more realistic description for the behavior of hydrogen atoms in close vicinity of the helium surface one has to rely on microscopic theories taking into account the detailed particularities of the surface region. Currently such theories are only available for impurities on the surface of liquid ^{4}He. Calculations were made by Mantz and Edwards [32], Guyer and Miller [16], and De Simone and Maraviglia [33]. Recently, Krotscheck et al. considered hydrogenic impurities on thin liquid ^{4}He films [34]. Here we discuss in some detail the extended Feynman–Lekner variational method employed by Mantz and Edwards to calculate the binding energy of H, D and T on liquid ^{4}He [35, 36, 32]. The method was developed with considerable success to describe ^{3}He impurities on the surface of ^{4}He. The method, being variational, should provide an upper limit for the energy and thus a lower limit for ε_a, its accuracy depends sensitively on input-knowledge of ground state properties of the ^{4}He surface, such as the density profile, the pair correlation function and the kinetic energy density near the surface. Also uncertainties and approximations of the interatomic pair potentials limit the accuracy of the method.

The Hamiltonian for a fluid of N ^{4}He atoms is given by

$$H_0 = -\frac{\hbar^2}{2m_4}\sum_{i=1}^{N}\nabla_i^2 + \tfrac{1}{2}\sum_{i\neq j}^{N} v_0(|\boldsymbol{r}_i - \boldsymbol{r}_j|)\ . \tag{3.7}$$

Here v_0 is the interatomic pair potential between helium atoms i and j. The ground-state wavefunction Ψ_0 satisfies the equation $H_0\Psi_0 = E_0\Psi_0$, where the ground state energy $E_0 = -NL_4$ if one neglects the surface contribution to the energy. The wavefunction Ψ_0 is symmetric under exchange of two atoms and may be taken to be real. The single-atom distribution function, which reflects the surface density profile of the liquid is defined by

$$n(\boldsymbol{r}_1) = N\frac{\int \Psi_0^2\ \mathrm{d}\boldsymbol{r}_{2-N}}{\int \Psi_0^2\ \mathrm{d}\boldsymbol{r}_{1-N}}\ . \tag{3.8}$$

If one ^{4}He atom, at position $\boldsymbol{r}_1$, is replaced by an impurity atom of mass

m the Hamiltonian for the modified system is

$$H = H_0 + \left(-\frac{\hbar^2}{2m} + \frac{\hbar^2}{2m_4} \right) \nabla_1^2 + \sum_{j=2}^{N} v_{\mathrm{d}}(|\boldsymbol{r}_j - \boldsymbol{r}_1|) \ , \tag{3.9}$$

where $v_{\mathrm{d}}(r) \equiv [v(r) - v_0(r)]$ accounts for the difference in pair-potential between the impurity–He pair and a He–He pair.

The Feynman trial wavefunction for liquid plus impurity is

$$\Psi(\boldsymbol{r}_1, \ldots, \boldsymbol{r}_N) = f(\boldsymbol{r}_1)\Psi_0(\boldsymbol{r}_1, \ldots, \boldsymbol{r}_N).$$

For our analysis we are in particular interested in the probability density $\rho(\boldsymbol{r}_1)$ of the impurity. In terms of the Feynman trial wavefunction, $\rho(\boldsymbol{r}_1)$ is given by

$$\rho(\boldsymbol{r}_1) = \frac{\int \Psi^2 \, \mathrm{d}\boldsymbol{r}_{2-N}}{\int \Psi^2 \, \mathrm{d}\boldsymbol{r}_{1-N}} = \frac{|f(\boldsymbol{r}_1)|^2 n(\boldsymbol{r}_1)}{\int |f(\boldsymbol{r}_1)|^2 n(\boldsymbol{r}_1) \, \mathrm{d}\boldsymbol{r}_1} \tag{3.10}$$

or, re-expressed in terms of a new function $\phi(\boldsymbol{r}_1) \equiv f(\boldsymbol{r}_1)\sqrt{n(\boldsymbol{r}_1)}$:

$$\rho(\boldsymbol{r}_1) = \frac{|\phi(\boldsymbol{r}_1)|^2}{\int |\phi(\boldsymbol{r}_1)|^2 \, \mathrm{d}\boldsymbol{r}_1}. \tag{3.11}$$

Notice that $\phi(\boldsymbol{r}_1)$ may be interpreted as the wavefunction of the impurity atom. To solve for $\phi(\boldsymbol{r}_1)$ Mantz and Edwards used the Feynman Lekner procedure, in which the function $f(\boldsymbol{r}_1)$ is varied in order to minimize the energy $\langle E \rangle = \langle \Psi | H | \Psi \rangle$ under the constraint $\langle \Psi | \Psi \rangle = 1$. This implies $\langle \delta\Psi | (H - E) | \Psi \rangle = 0$ [38], where E is the minimal energy. Taking variations only in $f(\boldsymbol{r}_1)$, the integral to be satisfied in minimizing the (undetermined) energy is

$$\int \mathrm{d}\boldsymbol{r}_1 \, \delta f \int d\boldsymbol{r}_{2-N} \, \Psi_0 (H - E) f \Psi_0 = 0 \ . \tag{3.12}$$

Using eqs. (3.9) and (3.8) and introducing the He–He two-body density distribution

$$n(\boldsymbol{r}_1, \boldsymbol{r}_2) = N(N-1) \frac{\int \Psi_0^2 \, \mathrm{d}\boldsymbol{r}_{3-N}}{\int \Psi_0^2 \, \mathrm{d}\boldsymbol{r}_{1-N}} \ , \tag{3.13}$$

eq. (3.12) may be re-expressed in the form of a Schrödinger equation for

$\phi(\boldsymbol{r}_1)$:

$$-\frac{\hbar^2}{2m}\nabla_1^2\phi(\boldsymbol{r}_1) + V_{\text{eff}}(\boldsymbol{r}_1)\phi(\boldsymbol{r}_1) = \varepsilon\phi(\boldsymbol{r}_1) \tag{3.14}$$

with

$$V_{\text{eff}}(\boldsymbol{r}_1) = -L_4 - \frac{\hbar^2}{2m}\left[\frac{1}{4}\left(\frac{\nabla_1 n}{n}\right)^2 - \frac{1}{2}\frac{\nabla_1^2 n}{n}\right] + \left(\frac{m_4}{m} - 1\right)\frac{t}{n}$$
$$+ \int \mathrm{d}\boldsymbol{r}_2\, n(\boldsymbol{r}_2)g(\boldsymbol{r}_1, \boldsymbol{r}_2)v_{\text{d}}(|\boldsymbol{r}_1 - \boldsymbol{r}_2|)\ ,$$

and

$$\varepsilon = (E - E_0 - L_4)\ .$$

Here $t(\boldsymbol{r}_1)/n(\boldsymbol{r}_1)$ is the kinetic energy per ^{4}He atom in the ground state

$$t(\boldsymbol{r}_1) = -\left(\frac{\hbar^2}{2m_4}\right) N \frac{\int \Psi_0 \nabla_1^2 \Psi_0\ \mathrm{d}\boldsymbol{r}_{2-N}}{\int \Psi_0^2\ \mathrm{d}\boldsymbol{r}_{1-N}}\ , \tag{3.15}$$

and $g(\boldsymbol{r}_1, \boldsymbol{r}_2)$ is the He–He pair correlation function for ^{4}He in its ground state, defined by

$$n(\boldsymbol{r}_1, \boldsymbol{r}_2) = g(\boldsymbol{r}_1, \boldsymbol{r}_2)n(\boldsymbol{r}_1)n(\boldsymbol{r}_2)\ . \tag{3.16}$$

Mantz and Edwards show explicitly how eq. (3.15) preserves the proper asymptotic behavior at long range.

Equation (3.14) describes the motion of the impurities in the effective field of an *undisturbed* helium background. Although the derivation strictly holds for the ground state, the same form should also hold for the excited states. Invoking strict translational symmetry the eigenstates may be written as

$$\phi_{\boldsymbol{k},\sigma}(\boldsymbol{R}, Z) = \mathrm{e}^{\mathrm{i}\boldsymbol{k}\cdot\boldsymbol{R}}\phi_\sigma(Z), \tag{3.17}$$

where $\boldsymbol{k}$ and $\boldsymbol{R}$ are the components of the wavevector and position of the atom parallel to the surface, Z is the distance to the surface reference plane and σ is the normal component of the atomic wavevector. For the bound state the notation $\sigma = B$ is used. The eigenvalues corresponding to

eq. (3.17) are given by

$$\varepsilon = \varepsilon_a + \hbar^2 k^2/2m \quad \text{(adsorbed states)}$$
$$\varepsilon = \hbar^2(k^2 + \sigma^2)/2m \quad \text{(continuum states)}. \tag{3.18}$$

In the present context ε_a is a lower limit to the binding energy. The wavefunction $\phi_\sigma(Z)$ is the solution to the one-dimensional analogue of eq. (3.14):

$$-\frac{\hbar^2}{2m}\frac{d^2\phi_\sigma(Z)}{dZ^2} + V_{\text{eff}}(Z)\phi_\sigma(Z) = \varepsilon_\sigma\phi_\sigma(Z)\ . \tag{3.19}$$

One refers to $V_{\text{eff}}(Z)$ as the surface adsorption potential. Further, $\varepsilon_\sigma = \varepsilon_a$ for the bound states and $\varepsilon_\sigma = \hbar^2\sigma^2/2m$ for the continuum states. In fig. 5 the adsorption potentials are shown for H, D, T, and ^{3}He along with the corresponding bound-state wavefunctions.

The adsorption potentials give rise to a single bound state in all four cases. At large distance above the surface the effective potentials of ^{3}He and H, D, and T differ only due to the v_d term in the expression for V_{eff}. Only in the bulk region $z \lesssim z_{\min}$, where $z_{\min}$ corresponds to the minimum in the effective potential for ^{3}He, do kinetic energy contributions lead to differences in the effective potentials. This causes the effective potentials for H, D, and T to be essentially identical in the region shown in fig. 5. Mantz and Edwards used the density profile proposed by Edwards and Fatouros, in which the density drops from 90% to 10% of the bulk value over a distance of 4.4 Å [37]. This surface thickness is considerable smaller than the more recent theoretical values presented by Stringari and Treiner [30].

Clearly the Feynman–Lekner scheme offers an elegant and powerful approach to the impurity problem on ^{4}He surfaces. It also has its weaknesses. From eq. (3.14) it is clear that the backflow effects, leading to the effective mass described in the previous section, are neglected. For the adsorbed state of H this is of little consequence as the bound state is located well above the liquid surface. Its principal weakness, however, is that all optimization is achieved by varying $f(\boldsymbol{r}_1)$, which means that correlations in the impurity–helium motion are treated as identical to He–He correlations in the pure liquid. More sophisticated approaches for the free surface, as carried out by Guyer and Miller, require other approximations that limit the overall accuracy [16]. The problems involved are not simple to overcome, as today, more than twelve years after publication, the results of Mantz and Edwards still stand out to provide best agreement with experiment. Monte Carlo schemes used by Krotscheck et al. to describe impurities on liquid helium film surfaces are most promising to improve the estimates for

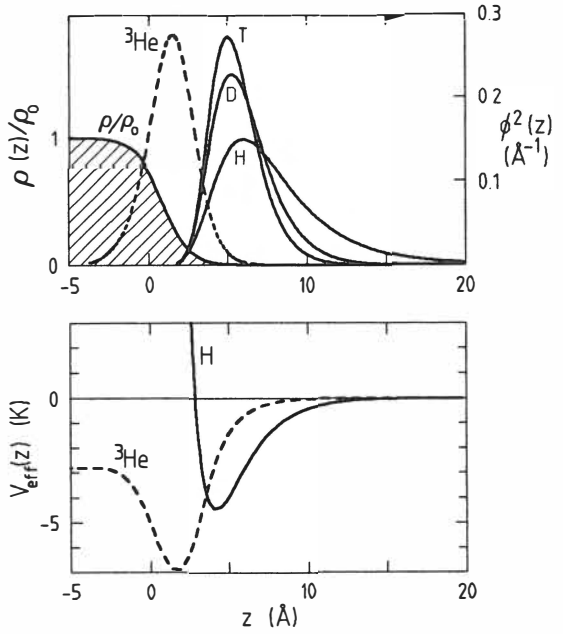

Fig. 5. Upper graph: density profile of the free surface of liquid ^{4}He as used by Mantz and Edwards and probability distributions of H, D, T, and ^{3}He impurities. The lower graph shows the effective potentials of H on ^{4}He (solid line) and that of ^{3}He on ^{4}He (dashed line).

both binding energies and bound-state wavefunctions [34].

3.3. The adsorbate as a dilute gas

In the preceding sections the properties of individual H atoms were examined in relation to the surface of liquid helium. For hydrogen *gas* in thermodynamic equilibrium with a helium surface many interesting additional aspects appear. There will be a rapid and continual exchange of atoms between bulk gas and surface and a steady-state density n_w of adsorbed atoms is established on the wall. The properties of this adsorbed state are largely independent of the detailed adsorption-desorption dynamics. We shall discuss some of the highlights of the adsorbed state before we turn in the next section to a discussion of the dynamical aspects of the gas–liquid interface. There are important advances in the microscopic theory of the adsorbed state of spin-polarized hydrogen. Although we have to skip many interesting details we shall discuss the prospects for a Kosterlitz-Thouless

(KT) transition in the adsorbed layer and two important consequences of this transition: the onset of 2D superfluidity and its effects on the surface adsorption isotherms.

In the adsorbed state, spin-polarized hydrogen may be considered a near-perfect realization of the weakly interacting two-dimensional (2D) Bose gas. For a given bulk density n_g the surface density may be varied by adjusting the temperature. As described by Silvera and Goldman [39] and by Edwards and Mantz [40], the surface density will increase exponentially with decreasing temperature until the repulsive interactions between the adsorbed atoms limit the density to a maximum value: the saturation density n_{sat}. It was pointed out by Edwards and Mantz that well before saturation is reached the adsorbed gas will undergo a Kosterlitz–Thouless (KT) transition to a superfluid state [41]. The critical temperature for this transition is

$$T_c^{2D} = (\pi\hbar^2/2mk_B)\, n_{sc} \ , \tag{3.20}$$

where $mn_{sc} \equiv \rho_{sc}$ is the superfluid mass density just below T_c^{2D} and m is the hydrogen mass. The current picture of the 2D Bose gas involves the existence of a quasi-condensate, a condensate with fluctuating phase, which has strong analogies with the concept of a Bose condensate in 3D. The concept of the quasi-condensate is due to Popov [43]. To estimate T_c^{2D}, n_{sc} has to be evaluated. At the critical temperature the superfluid fraction n_s/n_w changes discontinuously from zero to a finite value: n_{sc}/n_w [42]. The jump has been estimated to be close to unity [21, 44]. Thus, in numerical terms, to enter the KT regime at $T_c^{2D} = 100$ mK we find with eq. (3.20) that the surface density should exceed $n_w \approx 10^{13}$ cm^{-2} ($T/n_w \lesssim 7.6 \times 10^{-15}$ K cm^2). Unfortunately it is not possible to satisfy this condition for H gas in thermal equilibrium with a helium surface. Three-body dipolar recombination will lead to unmanageable heating of the sample. However, by cooling a small section of a liquid helium covered sample cell to a temperature much lower than its surroundings it should be possible to study the KT regime in steady state [45]. This is one of the open challenges for the experimentalists in the field.

To evaluate how well the weakly interacting Bose picture applies to the adsorbed state of hydrogen on liquid helium we introduce two characteristic temperatures, the degeneracy temperature $\tilde{T}$ and the temperature T^* associated with the elastic interactions between the atoms. The gas is weakly interacting if the interactions may be treated perturbatively. In practice this is the case for $T^* \ll \tilde{T}$. From very general considerations the onset of quantum degeneracy is to be expected when the distance be-

tween atoms approximately equals the thermal de Broglie wavelength Λ. Then, a description in terms of atoms represented by wavepackets breaks down due to mutual overlap and should be replaced by a description with a properly symmetrized many-body wavefunction. For 3D this criterion implies degeneracy for $T \lesssim \tilde{T}_g \equiv (2\pi\hbar^2/mk_B)n_g^{2/3}$. In a non-degenerate dilute gas the actual transition (BEC) occurs at a slightly lower temperature: $T_c^{3D} = 3.31(\hbar^2/mk_B)n_g^{2/3}$. For 2D the degeneracy temperature is

$$\tilde{T}_w \equiv (2\pi\hbar^2/mk_B)\, n_w. \tag{3.21}$$

Before we turn to the interactions in the adsorbate we briefly mention for comparison some properties of the bulk gas. Many more bulk properties are summarized in the lectures by Greytak and Kleppner [1]. The 3D elastic interaction energy is well-known from textbook treatments of the weakly interacting Bose gas [58]. At $T = 0$ K the energy per particle and condensate fraction are given by

$$E_g/N = \tfrac{1}{2} n_g V_g^* [1 + O(\xi_g)], \tag{3.22}$$

$$n_g^0/n_g = 1 - \tfrac{8}{3}(1/\pi)^{1/2}\xi_g\,, \tag{3.23}$$

where $V_g^* = (4\pi\hbar^2/m)\, a_s$ is the scattering strength and the expansion parameter is defined by $\xi_g \equiv (n_g a_s^3)^{1/2}$. The low-density regime defined by $\xi_g \ll 1$ is know as the dilute limit. The expansion (3.22) is only meaningful if the s-wave scattering length a_s is positive. For $a_s < 0$ the gas is instable against formation of a many-body bound state (liquid). For two H-atoms interacting via the triplet potential Friend and Etters calculated $a_s = 0.72$ Å[47]. This corresponds to $V_g^* = 4.4 \times 10^{-22}$ K cm^3. The chemical potential is given by

$$\mu_g = (\partial E_g/\partial N)_V = n_g V_g^*\,. \tag{3.24}$$

With the definition $n_g V_g^* \equiv k_B T_g^*$ we find $T_g^* = n_g(4\pi\hbar^2/mk_B)\, a_s$ for the interaction temperature. Combining the expressions for T_g^* and $\tilde{T}_g$ one finds that the ratio of the characteristic temperatures is closely related to the expansion parameter: $\xi_g = \frac{1}{4}\sqrt{2}(T_g^*/\tilde{T}_g)^{3/2}$. Notice further that even for the highest bulk densities of experimental interest, $n_g \approx 10^{20}$ cm^{-3}, the dilute gas approximation is very well satisfied ($T_g^*/\tilde{T}_g \approx 0.07$) and the condensate fraction at $T = 0$ K is expected to be approximately 99%.

Elastic scattering in 2D is void of the simple low-energy limit that is known from 3D effective range theory. In 3D the s-wave scattering length

a_s has a special significance because the cross section has a well-defined low-energy limit: $\sigma(k) = 8\pi a_s^2$. In 2D it is also possible to formulate a proper effective range theory, mapping the problem onto hard discs of diameter a (the 2D scattering length). However, the scattering of hard discs has a non-trivial low-energy limit in the sense that the 2D total cross section (cross-length) diverges for small relative momenta, while the scattering rate is vanishing logarithmically.

A critical discussion of 2D effective range theory was published by Verhaar et al. [48], who give the following expression for the phase shift

$$\operatorname{cotan} \eta_0(k) = \frac{2}{\pi}(\gamma + \ln \tfrac{1}{2}ka) + \frac{1}{2\pi} r_e^2 k^2, \tag{3.25}$$

where a and r_e are the 2D scattering length and effective range, respectively; $\gamma = 0.577\,215\,665\ldots$ is the Euler constant. For two H-atoms on the surface of ^{4}He interacting via the triplet potential the 2D scattering length $a \approx 0.9$ Å was first established by Kagan et al. [49]. The estimates of Verhaar et al. [48, 50] for scattering length and effective range are $a = 2.3\,a_0$ and $r_e = 14.3\,a_0$. A more compact but less accurate expression for the phase shift is given by Schick [51] in his article on the hard disc Bose system:

$$\sin \eta_0 = -\tfrac{1}{2}\pi / \ln ka, \quad ka \ll 1. \tag{3.26}$$

Equation (3.26) overestimates the phase shifts in adsorbed hydrogen by at most 20% for energies less than 0.5 K [48]. The divergence of the 2D total cross section for $ka \ll 1$ follows directly with eq. (3.26) and $\sigma(k) = (4/k)\sin^2 \eta_0$ [51]. Multiplying the cross section with the thermal velocity to obtain the scattering rate, this quantity is seen to vanish logarithmically as mentioned before. In 2D the scattering length is always positive and therefore not indicative for the attractive or repulsive character of the interactions.

Schick gives expressions for the ground-state energy per particle and the condensate fraction of a many-body system of hard-disc Bosons in the dilute limit:

$$E_w/N = \tfrac{1}{2} n_w V_w^* [1 + O(\xi)] \tag{3.27}$$

$$n_w^0/n_w = 1 - \xi + O(\xi^2) \tag{3.28}$$

where $V_w^* = (4\pi\hbar^2/m)\,\xi$ is the scattering strength with $\xi^{-1} \equiv -\ln(n_w a^2)$. The validity of eq. (3.27) for the hard disk Bose gas is analyzed in detail

by Bruch, who also extends the expansion to include the second order term [52]. From eq. (3.27) and eq. (3.22) the interaction energy is seen to be positive for all densities, both in the bulk and on the surface. This means that spin-polarized hydrogen confined by helium covered surfaces remains gaseous down to $T = 0$ K. The practical limitations on the stability are caused by the chemical reactivity of the samples, in particular three-body dipolar recombination [2], and not by instabilities leading to a liquid (or solid) ground state. Writing $\mu_w = (\partial E_w/\partial N)_A = n_w V_w^* \equiv k_B T_w^*$ the characteristic temperature associated with the elastic interactions within the adsorbate is

$$T_w^* \equiv n_w(4\pi\hbar^2/mk_B)\,\xi\,. \tag{3.29}$$

The ratio of the characteristic temperatures is found to be $T_w^*/\tilde{T}_w = 2\xi$, showing for the 2D case the close relation with the expansion parameter. For surface densities $n_w = 10^{13}$ cm^{-3}, the expansion parameter $\xi = 0.15$ and $V_w^* = 9 \times 10^{-15}$ K cm^2 as the reader may verify by substituting the value of the 2D scattering length in the expression for ξ. Thus the weakly interacting gas picture is seen to be valid, be it not as good as in 3D. For wall densities $n_w = 10^{14}$ cm^{-3} the second term in the Bruch expression for the ground state energy (see ref. [52]) contributes on a 30% level. It is typical for the 2D case that variation of the density has little effect on the validity of the dilute gas approximation. This originates in the weak density dependence of ξ. One easily verifies that for the large range of densities $n_w = 10^{12} - 10^{14}$ cm^{-3}, the relation

$$T_w^* \approx T_c^{2D} \approx \tfrac{1}{4}\tilde{T}_w \tag{3.30}$$

is valid to within an accuracy of 50%. In particular Kagan and collaborators used the theory of the weakly interacting 2D Bose gas to systematically analyze the collective properties of hydrogen adsorbed on liquid helium [49, 44, 53]. Other papers discussing the onset of superfluidity in weakly interacting Bose films are by Saam [54] and by Shevchenko [55]. A useful paper making the link to the work of Popov [43] was written by Fisher and Hohenberg [56].

3.4. Variational calculations

Historically, the first calculations of the energy per particle in the adsorbate were done with a variational method by Miller and Nosanow [57]. These authors used a Jastrow type variational wavefunction, using a Lennard-Jones fit to the triplet potential and assuming a strictly 2D motion. The

variational approach is accurate to higher densities than the dilute gas approach presented in the previous section. Miller and Nosanow found a linear density dependence for the ground state energy per particle. Using their results one may extract $V_w^* = 1.9 \times 10^{-14}$ K cm^2 for the effective scattering strength. Lantto and Nieminen [58] and also Silvera and Goldman [39] used the triplet potential directly in numerical calculations and found $V_w^* \approx 1.3 \times 10^{-14}$ K cm^2.

Miller and Nosanow point to the absence of logarithmic terms in their results, which is at variance with the perturbative treatment of Schick, but its significance remains unclear. Bruch [52] also addresses this point for finite-range potentials and shows that (in the absence of two-body bound states) variational treatments with Jastrow-type trial functions have the capacity to produce the nonlinear density dependence of eq. (3.27). He arrives at the assertion that eq. (3.27) represents the correct form for the ground-state energy in 2D. It is of course not obvious that this conclusion remains unchanged if the spatial extend of the bound-state wavefunction is taken into account. We briefly return to this point in the next section. Here we do not enter into the details of the Jastrow-variational method but merely emphasize the level of agreement between the variational results and those of eq. (3.27) as another indication for the validity of the weakly interacting gas picture.

3.5. Quasi-two-dimensional or quasi three-dimensional behavior?

What are the consequences of the limited two-dimensionality of the adsorbed state? In section 3.2 it was shown that the bound-state wavefunction extends ~10 Å above the surface and it is not obvious that this may be simply discarded. To elucidate some of these aspects, consider a pair of H-atoms adsorbed on the surface of liquid helium and mutually interacting through the b-$^3\Sigma_u^+$-potential $V_t(r)$, neglecting magnetic interactions. Except for providing the effective adsorption potential the surface will be ignored. The motion of the individual atoms is described by eq. (3.17), which means that the motions parallel and normal to the surface are uncorrelated. For two adsorbed atoms these degrees of freedom are coupled by the mutual interaction. This makes collisions on the surface, at least in principle, into a highly anisotropic 3D scattering phenomenon. However, the normal motion is very fast in comparison to the relative motion in the plane of the surface, suggesting an approximation in which the problem may be reduced to a quasi-2D problem by averaging the quantities of interest over the bound-state wavefunction. The validity of this approximation was analyzed in detail by van den Eijnde et al. ($2\frac{1}{2}$D-approximation)

who found it to be very good to describe magnetic relaxation problems on the surface [59]. The relative motion of the pair is analyzed in terms of 2D partial waves, writing the 3D pair wavefunction on the surface as

$$\Psi(\rho, Z_1, Z_2) = \sum_m \rho^{-1/2} F_m(\rho, Z_1, Z_2)\, \mathrm{e}^{im\phi} \,. \tag{3.31}$$

Approximating $F_m(\rho, Z_1, Z_2)$ by $\phi_0(Z_1)\phi_0(Z_2)y_m(\rho)\exp(im\phi)$ the variables are separated. Here $\rho \equiv \boldsymbol{R}_1 - \boldsymbol{R}_2$ and $\phi_0(Z)$ is the bound-state wavefunction, real and normalized to unity and defined by eq. (3.19). Within this approximation the Schrödinger equation for the pair (in cylindrical coordinates) can be reduced to

$$\left[\frac{\partial^2}{\partial\rho^2} + \frac{1}{4}\frac{(1-4m^2)}{\rho^2} - U(\rho, z) - 2U_\mathrm{a} + k^2\right] \phi_0(Z_1)\phi_0(Z_2)y_m(\rho) = 0,$$

in which $z \equiv Z_1 - Z_2$, $U(r) \equiv (2\mu/\hbar^2)V_\mathrm{t}(r)$, $k^2 \equiv (2\mu/\hbar^2)E$ and $U_\mathrm{a} \equiv (2\mu/\hbar^2)\varepsilon_\mathrm{a}$. The symbol μ is used here locally to indicate the reduced mass of the pair. Multiplying the left-hand side with $\phi_0(Z_1)\phi_0(Z_2)$ and integrating over Z_1 and Z_2, one arrives at the 2D radial equation

$$\left[(\mathrm{d}^2/\mathrm{d}\rho^2) + \tfrac{1}{4}(1-4m^2)/\rho^2 - U(\rho) + k^2\right] y_m(\rho) = 0 \,, \tag{3.32}$$

where the zero of energy has been shifted by $2\varepsilon_\mathrm{a}$ and the effective 2D potential is defined by $U(\rho) \equiv \int \mathrm{d}Z_1 \int \mathrm{d}Z_2\, \phi_0^2(Z_1)\phi_0^2(Z_2)U(\rho, z)$. The latter expression may be expressed more compactly in terms of the distribution function $F(z)$

$$U(\rho) = \int U(\rho, z)F(z)\, \mathrm{d}z, \tag{3.33}$$

$$F(z) \equiv \int \phi_0^2\left(Z + \tfrac{1}{2}z\right) \phi_0^2\left(Z - \tfrac{1}{2}z\right)\, \mathrm{d}Z, \tag{3.34}$$

with $Z \equiv \frac{1}{2}(Z_1 + Z_2)$. The average probability density in the bound state $F(0) = 0.095$ Å^{-1} was first determined by Edwards and Mantz [40]. Verhaar and coworkers replaced $F(z)$ by a Gaussian and found a slightly larger value for $F(0)$ to be the best choice (in comparison to a full 3D analysis) to calculate magnetic relaxation rates [59]. The replacement $F(z) = \delta(z)$ yields the pure 2D approach referred to in section 3.4

There is also another approach to the problem. As suggested by Edwards and Mantz one may argue that the localization of the atoms to the surface is

in fact rather poor and that the adsorbate resembles a thin film with certain bulk-like properties rather than a strictly 2D system [40]. Such a quasi-3D approach is allowed if the pair correlation at short distance is 3D like, i.e., for $r_0 \ll l$, where $r_0 = 3.68$ Å is the hard-core diameter (see section 2.2) of the interaction potential and l is a localization length related to the spatial extent of the bound-state wavefunction. Etters et al. [60] and Lantto and Nieminen [61] show 3D pair correlation functions for several densities. The quasi-3D energy per particle takes the form

$$E_w/N = \int \tfrac{1}{2} n_w^{3D}(Z) V_g^* \phi_0^2(Z)\, dZ\,, \tag{3.35}$$

where $n_w^{3D}(Z) = n_w \phi_0^2(Z)$ is the density distribution in the surface layer. With eq. (3.34), eq. (3.35) reduces to $E_w/N = \frac{1}{2} n_w V_g^* F(0)$, so that from a comparison with eq. (3.27) we find with eq. (3.34)

$$V_w^* = (4\pi\hbar^2/m)\, a_s F(0)\,. \tag{3.36}$$

It is instructive in this context first to have a look how big the average effective 3D-densities $\langle n_w^{3D}(Z)\rangle$ in the adsorbate actually are. For a surface coverage $n_w = 10^{13}$ cm^{-2} one calculates $\langle n_w^{3D}(Z)\rangle = n_w F(0) \approx 10^{20}$ cm^{-3} with the procedure of eq. (3.35). Such an effective density would correspond to a bulk transition temperature (BEC) of ~ 350 mK. It is consistent with the picture of the Kosterlitz and Thouless that due to vortex pair breaking the actual transition should occur at a lower temperature ($\sim$ 100 mK) as estimated in section 3.3. Comparing the quantity $a_s F(0) = 0.07$ in eq. (3.36) ($V_w^* = 4.3 \times 10^{-15}$ K cm^2) with the expansion parameter $\xi = 0.15$ introduced in section 3.3, one observes that the interaction strength for the quasi-3D model is again of the same order of magnitude as found for the previously discussed models, although with the approximation the logarithmic density dependence is lost. The latter is not the case in the analysis of Kagan et al. [49, 44] who used an approach similar to that of Edwards and Mantz, but with a simple approximation to the bound-state wavefunction that enables analytical results:

$$\phi_0(Z) = (2/l)^{1/2} \exp(-Z/l)\,, \tag{3.37}$$

where $l = (\hbar^2/2m\varepsilon_a)^{1/2}$. For adsorption on ^{4}He this implies $l \approx 5$ Å. Within this approximation and further assuming that $r_0 \ll l$ (which is not very well satisfied for H on ^{4}He) they derive for the low-k limit an analytic expression for a parameter $a^* = (l/2)\exp(-l/2a_s)$, which replaces

the 2D scattering length. The corresponding scattering amplitude has the form $V_w^*(k) = (4\pi\hbar^2/m)\,\xi^*$, with $\xi^{*-1} = -\ln(k^2 a^{*2})$ and hence logarithmic character for small k is conserved. Numerically we find $a^* \approx 0.15\,a_0$, which is much smaller than the $2.3\,a_0$ found by Verhaar et al. [48]. Possibly this is associated with limits to the validity of the derivation for the particular case of an H adsorbate on ^{4}He. For ^{3}He or ^{3}He/^{4}He mixture surfaces $l \approx 8$ Å and the approximation should work better. Aside from these considerations the logarithmic dependence on a^* assures that the numerical consequences for V_w^* remain small.

In summary, the weakly interacting picture is seen to hold fairly well for H adsorbed on liquid helium. The numerical value obtained for the scattering strength, $V_w^* \approx 10^{-14}$ K cm^2, turns out to be not very sensitive to the particular model used to describe the adsorbate. In detail, the strictly 2D models (which are most restrictive for the motion of the atoms) lead to the highest values for V_w^*. The less restrictive quasi-3D approach results in an effective interaction strength which is a factor 2 -3 smaller.

3.6. The surface adsorption isotherms and KTT

The surface adsorption isotherm is the relationship between n_w and n_g for a gas in thermal equilibrium with a surface. It is obtained by equating the chemical potentials of bulk gas (μ_g) and the adsorbate (μ_w). For $T = 0$ K the situation is very simple. Feeding atoms into a volume bounded by helium covered walls, all atoms will be confined to the surface until the chemical potential of the adsorbate, $\mu_w = n_w V_w^* - \varepsilon_a$, equals zero and the bulk starts to be populated. Thus, the $T = 0$ K saturation density is

$$n_w^{sat} = \varepsilon_a / V_w^* \approx 10^{14}\ \text{cm}^{-2}, \tag{3.38}$$

as was realized in all early papers on this subject.

For $T > 0$ K the interaction energy per unit density changes. In mean field theories, symmetrization causes elementary scattering processes by pairs of particles in different states to contribute twice to thermodynamic averages where particles in the same state contribute only once. Hence, per unit density the interaction energy of the condensate particles is a factor 2 smaller than that of above-condensate particles. Since in 2D a condensate is rigorously absent at finite temperatures, Goldman and Silvera argued that the saturation density in any physically realizable system should be a factor 2 smaller than the value given in eq. (3.38) [62]. This point was carried in subsequent reviews [21, 1, 2]. Later, Kagan et al. [44] have pointed out that although for $T > 0$ K the long-range order is destroyed and it is

impossible to define a single condensate wavefunction for the entire system, still in any local environment it is possible to define a quasi-condensate in which a macroscopic number of particles participate and for which the symmetrization requirement leads to essentially the same mean field as for $T = 0$ K. The participation of many particles assures that the density fluctuations of the quasi-condensate are small. The correlation length is given by [44]

$$R_c = \left(\frac{T_w^*}{T_w}\right) r_c \exp\left(\frac{1}{\alpha}\right); \qquad \alpha = \frac{m n_w}{\rho_s}\frac{T_w}{T_w^*}\xi, \tag{3.39}$$

where $\rho_s = m n_s$ is the superfluid mass density. Notice that R_c diverges for $T \to 0$. In the absence of vorticity this quasi-condensate persists up to $T_w \approx \tilde{T}_w$ and (as $T_w^{2D} \approx \frac{1}{4}\tilde{T}_w$) in fact involves a major fraction of the adsorbate for $T_w < T_c^{2D}$. According to the theory of Kosterlitz and Thouless above T_c^{2D} free thermal vortices appear and ρ_s rapidly drops to zero. As a consequence, the change by a factor ~2 in the interaction energy. mentioned above, should be expected at the Kosterlitz Thouless transition and not at $T = 0$ K. This is discussed in the paper of Svistunov et al. [45].

At finite temperatures also a thermal contribution has to be added to the chemical potentials of bulk and surface. For the ideal 2D and 3D Bose gas one has the well-known relations

$$n_g = n_0 + \Lambda^{-3} g_{3/2}(z); \qquad n_w = \Lambda^{-2} g_1(z), \tag{3.40}$$

where the fugacity expansions $g_n(z) \equiv \sum_{l=1}^{\infty} z^l/l^n$ with $z \equiv \exp(\mu/k_B T)$, define the usual Bose integrals in the absence of spin degeneracy [63]. The expressions allow for a Bose condensate of density n_0 in the bulk. A condensate term does not appear in the expression for n_w because for a homogeneous system in two dimensions a real condensate is rigorously absent except at $T = 0$ [64]. Thus

$$\mu_{id}^{3D} \approx k_B T \ \ln(n_g \Lambda^3), \quad \text{for } T_g > \tilde{T}_g, \tag{3.41}$$

$$\mu_{id}^{3D} = 0, \quad \text{for } T_g \leqslant T_c^{3D}, \tag{3.42}$$

$$\mu_{id}^{2D} = k_B T \ \ln[1 - \exp(-n_w \Lambda^2)]. \tag{3.43}$$

In the presence of interactions the excitation spectrum fundamentally changes. The Bose symmetrization requirement only allows collective excitations in a system with a condensate. In the usual description for the weakly interacting Bose gas, due to Bogoliubov, the excitations behave as

an ideal gas of quasi-particles which cannot be identified with the individual gas atoms [65]. This has little consequence for μ_g. Except for extremely low temperatures ($T_g < T_g^*$), the thermal kinetic energy is stored predominantly in free-particle-like excitations and since $T_g^* \ll \tilde{T}_g$ the expressions for the 3D ideal Bose gas suffice to predict T_c^{3D}. For 2D the situation is different. Since in 2D $T_w^* \approx T_c^{2D} \approx \frac{1}{4}\tilde{T}_w$ as we saw in section 3.3, the expressions for the ideal 2D Bose gas can only be used for $T_w > T_c^{2D}$. For the Kosterlitz Thouless regime the proper excitation spectrum should be used to calculate the chemical potential [43].

As our interest concerns here in particular the KT transition region, we choose to analyze the adsorption well below the critical density for BEC in the bulk, thus enabling an analytical expression for the chemical potential in 3D

$$\mu_g \approx k_B T \ln(n_g \Lambda^3) + 2 n_g V_g^*, \quad \text{for } T > \tilde{T}_g, \tag{3.44}$$

$$\mu_w = -\varepsilon_a + n_w V_w^* \{1 + \xi[f(T/T_w^*) + O(\ln|\xi|)]\}, \quad \text{for } T < T_w^{2D}, \tag{3.45}$$

$$\mu_w = \mu_{id}^{2D} - \varepsilon_a + 2 n_w V_w^*, \quad \text{for } T > T_w^{2D}. \tag{3.46}$$

The function $f(x)$ describes the temperature dependence of μ_w. It is given explicitly by Svistunov et al. [45]. Its presence in eq. (3.45) is of little consequence as $\xi \approx 0.15$ and $f(x) < 1$ for $T \leqslant T_c^{2D}$ [45]. Equating μ_g and μ_w the surface adsorption isotherms are obtained. In fig. 6 the results for the $T = 0.1$ K and $T = 0.3$ K isotherms are shown. In the KT transition region the drop in interaction energy leads to an increase in surface density by a factor $\sim$2.

Analyzing the steady-state properties of the 2D gas two regimes may be distinguished. In a high-temperature regime the steady-state density is the result of a balance between particle gain by adsorption and particle loss by desorption. At low temperatures the desorption rates become very small and particle loss is dominated by recombination. Under the latter conditions the adsorption isotherms defined by eq. (3.46) are no longer valid.

4. Collisions of H-atoms with the surface of liquid helium

In general, when H-atoms collide with the surface of liquid helium a variety of processes may take place. The atoms may simply scatter off elastically, leaving the surface unperturbed, or excite the surface creating ripplons or phonons, while adsorbing or scattering off non-specularly. In the coming

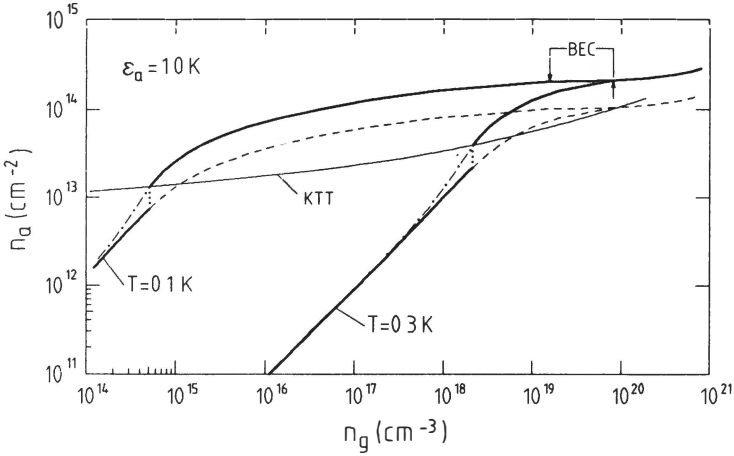

Fig. 6. Adsorption isotherms of H on ^{4}He for two different temperatures (fat solid curves). The intersection of the isotherms with the thin solid curve defines the KT transition points. The dashed lines are the isotherms (with exchange contribution) given by Goldman and Silvera. Note the cross-over to the dash-dotted curves (no exchange) at the KT-transition.

sections the most relevant scattering phenomena will be discussed within the framework developed up to this point, putting emphasis on the low-energy limit. Rather than switching formalism all scattering channels will be discussed within one and the same perturbative approach.

From a general point of view the choice of atom and surface is rather specialized. Nevertheless, many of the features to be described are typical for any surface collision at vanishing incident energy. In this sense the H He system may be regarded as a model system. In view of its small mass the quantum limit is reached with hydrogen at relatively high energies, while the exceptionally weak atom surface interaction enables an accurate description in terms of low-order perturbation theory, except in the vicinity of resonances in the adsorption potential.

4.1. The elementary excitations of the ^{4}He surface: ripplons

Aiming at a description of inelastic scattering phenomena of H-atoms with liquid helium surfaces we first briefly review the intrinsic excitations of those surfaces. As little is known of the excitations on ^{3}He the present discussion is restricted to liquid ^{4}He surfaces. Further, we shall not discuss

here the microscopic theory of these excitations, but rather present a phenomenological theory in terms of collective excitations in which the liquid is treated as an incompressible non-viscous fluid and the surface profile is a step function in the density. This approach is due to Atkins [66]. For a discussion of many more aspects of helium surfaces the review paper by Edwards and Saam is recommended [37].

For our purpose we consider a layer of pure liquid ^{4}He of thickness d covering a horizontal planar substrate. For d being small ($d \lesssim 200$ Å) one deals with properties of a helium film. In the limit $d \to \infty$ the layer behaves as bulk liquid and the properties of the free surface should be eminent. The fluid layer will support wave-like hydrodynamic modes, which will experience very little damping as ^{4}He is a superfluid. The elementary excitations of the helium surface are known as ripplons, quantized capillary waves [66]. They are related to fluctuations in the thickness of the liquid layer

$$h(\boldsymbol{r}) = A^{-1/2} \sum_{\boldsymbol{q}}^{\boldsymbol{q}_{\max}} h_{\boldsymbol{q}} \, \mathrm{e}^{\mathrm{i}\boldsymbol{q}\cdot\boldsymbol{r}} \, , \tag{4.1}$$

where $\boldsymbol{r}$ is a position vector in the plane of the undisturbed surface and

$$h_{\boldsymbol{q}} = \left(\frac{\hbar q \tanh(qd)}{2\rho_0 \omega_q}\right)^{1/2} (r_{\boldsymbol{q}}^{+} + r_{-\boldsymbol{q}}) \tag{4.2}$$

is the ripplon amplitude operator. Notice that the commutator $[h_{\boldsymbol{q}}, h_{\boldsymbol{q}'}] = 0$ for all $\boldsymbol{q}$ and $\boldsymbol{q}'$. The summation in eq. (4.1) is restricted to wavenumbers $\boldsymbol{q} \lesssim \boldsymbol{q}_{\max}$, as for wavelengths smaller than the interatomic spacing of the liquid the continuum picture breaks down ($q_{\max} \approx 1$ Å^{-1}). Further, $r_{\boldsymbol{q}}^{+}$ and $r_{\boldsymbol{q}}$ are creation and annihilation operators for ripplons with wavevector $\boldsymbol{q}$ in the plane of the surface, $\rho_0 = m_4 n_4$ is the ground-state mass-density of ^{4}He, as in section 3.1, and ω_q is related to q by the dispersion relation

$$\omega_q^2 = [g_{\mathrm{eff}} q + (\gamma/\rho_0) q^3] \tanh(qd), \tag{4.3}$$

shown in fig. 3. The ripplon dispersion is composed of two contributions. The first term in eq. (4.3) results from a gravity-like restoring force, characterized by an acceleration

$$g_{\mathrm{eff}} = g + \frac{3\alpha_3}{m_4 d^4} \, , \tag{4.4}$$

where α_3 is the van der Waals parameter of the interaction experienced

by a ^{4}He atom at a distance z above the substrate: $U(z) = -\alpha_3/z^3$. For a helium film of thickness $d = 100$ Å on a quartz substrate ($\alpha_3 = 1.62 \times 10^{-50}\,\mathrm{kg\,m^5\,s^{-2}}$) this van der Waals contribution is 10^8 times larger than the real gravity contribution, so that gravity effects may be neglected except for liquid layers of thickness $d \gtrsim 1$ μm. The second term in the dispersion relation is associated with surface tension (γ) as a restoring force. For ^{4}He the surface tension is given by $\gamma(T) = \gamma_0 - \gamma_1 T^{7/3} - \gamma_2 T^5$, where $\gamma_0 = 3.54 \times 10^{-4}$ J m^{-2} is the value at $T = 0$ K, $\gamma_1 = 6.5 \times 10^{-6}$ J m^{-2} K$^{-7/3}$ and $\gamma_2 = 6.3 \times 10^{-7}$ J m^{-2} K^{-5} [67]. From eq. (4.3) one notices that for long-wavelength ripplons the gravity-like term is dominant. The cross-over wavelength

$$\lambda_0 = 2\pi \left(\frac{\gamma}{g_{\mathrm{eff}} \rho_0} \right)^{1/2} \approx 2\pi d^2 \left(\frac{\gamma}{3\alpha_3 n_4} \right)^{1/2} \tag{4.5}$$

depends quadratically on the film thickness. For $d = 100$ Å one calculates $\lambda_0 \simeq 3600$ Å. The hyperbolic tangent in eqs. (4.2) and (4.3) accounts for effects associated with the layer thickness. For small ripplon wavelength ($\lambda \ll d$) it does not influence the dispersion of the waves. For wavelengths much larger than the film thickness the wave senses the substrate and the dispersion is modified by a factor qd.

It is a useful exercise to estimate which ripplons may be thermally excited. Statistically the ripplons behave as bosons, with the ripplon occupation being given by

$$n_{\boldsymbol{q}} = \frac{1}{\exp(\hbar\omega_{\boldsymbol{q}}/k_{\mathrm{B}}T) - 1} \tag{4.6}$$

Thus, for frequency much higher than that of the thermal ripplon, defined by $\hbar\omega_q = k_{\mathrm{B}}T$, the thermal occupation vanishes. For low-frequency excitations $\hbar\omega_q \ll k_{\mathrm{B}}T$ the quasi-classical expression applies:

$$n_{\boldsymbol{q}} \approx k_{\mathrm{B}}T/\hbar\omega_q \,. \tag{4.7}$$

For thick films under conditions where the surface tension term is dominant, the wavelength of the thermal ripplon is given by

$$\lambda_T T^{2/3} = 2\pi \left(\frac{\gamma\hbar^2}{\rho_0 {k_{\mathrm{B}}}^2} \right)^{1/3} \tag{4.8}$$

A thick film is defined in this context by $d \gg \lambda_T$. At 200 mK this cor-

responds to $\lambda_T = 95$ Å. This means that dynamic surface roughness on a smaller scale solely arises from the presence of zero-point fluctuations.

We next estimate the typical mean square fluctuation $\langle h^2 \rangle$ of the surface due to ripplons using the method presented by Cole [68]. The mean square displacement is defined by

$$\langle h^2 \rangle = \langle \langle h^2(\boldsymbol{r}) \rangle \rangle \ , \tag{4.9}$$

where $\langle\langle\ \rangle\rangle$ denotes the quantum-statistical average. Since we are looking for an expectation value, which is a diagonal property, eq. (4.9) may be rewritten with the aid of eq. (4.2) as

$$\langle h^2 \rangle = A^{-1} \sum_{\boldsymbol{q}}^{\boldsymbol{q}_{\max}} \langle \langle h_{\boldsymbol{q}} h_{-\boldsymbol{q}} \rangle \rangle = A^{-1} \sum_{\boldsymbol{q}}^{\boldsymbol{q}_{\max}} \frac{\hbar q \tanh(qd)}{2\rho_0 \omega_q} \langle \langle 1 + 2\hat{n}_q \rangle \rangle \ , \tag{4.10}$$

where $\hat{n}_q = r_{\boldsymbol{q}}^{+} r_{-\boldsymbol{q}}$ is the number operator. This expression contains two contributions. The first contribution is due to the zero-point motion. With the usual continuum transition $\sum_{\boldsymbol{q}} \to A/(2\pi)^2 \int \mathrm{d}\boldsymbol{q}$ it becomes:

$$\langle h_1^2 \rangle = \frac{\hbar}{4\pi\rho_0} \int_0^{\boldsymbol{q}_{\max}} \left(\frac{q^2}{\omega_q} \right) \tanh(qd)\ \mathrm{d}q \approx \frac{\hbar \omega_{\max}}{6\pi\gamma} \ , \tag{4.11}$$

provided $\lambda_{\max} \ll d$. Similarly one finds for the second contribution which arises from the thermal excitations:

$$\langle h_2^2 \rangle = \frac{\hbar}{2\pi\rho_0} \int_0^{\infty} \frac{q^2}{\omega_q} n_q \tanh(qd)\ \mathrm{d}q = \frac{k_{\mathrm{B}} T}{3\pi\gamma} f_0 \ln \left(\frac{k_{\mathrm{B}} T}{\hbar \omega_0} \right) \tag{4.12}$$

with $\omega_0^2 \simeq g_{\mathrm{eff}} q_0 \tanh(qd)$. The parameter $f_0 = 1$ for bulk helium and $f_0 = 3/4$ for films with $\lambda_T \gg d$. The rms fluctuations are plotted in fig. 7 both for the free surface of liquid helium and for a helium film of 100 Åon a quartz substrate. As an aside it is interesting to note that the low-frequency cutoff arises from the presence of the gravity contribution to the dispersion. Without this term the surface fluctuations diverge at any finite temperature. The strong enhancement of g_{eff} in the case of films is seen to strongly suppress the thermal fluctuations.

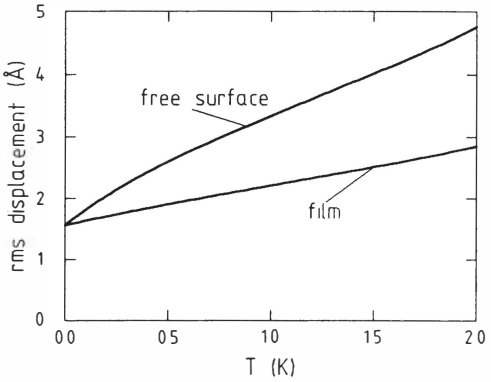

Fig. 7. The rms displacement of the surface of ^{4}He under its saturated vapor pressure as a function of temperature. Note the strong suppression of the thermal fluctuations in the case of films.

4.2. Atom–ripplon coupling

To analyze explicitly how the presence of ripplons affects the H–He atom surface interaction consider an H-atom at position $(\boldsymbol{R}, Z)$ above a bulk quantity of liquid ^{4}He as illustrated in fig. 8. The ^{4}He atomic coordinates are denoted by $(\boldsymbol{r}, z)$ and $h(\boldsymbol{r})$ represents the z-position of the interface at site $\boldsymbol{r}$. An ansatz for the interaction between atom and liquid is obtained by integrating the H He interatomic potential, $V(|\boldsymbol{R} - \boldsymbol{r}|^2 + |Z - z|^2)$, over the volume of the liquid, while assuming the potentials to be pairwise

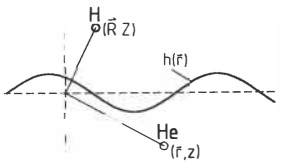

Fig. 8. The coordinate system in which the atom- surface interaction is analyzed.

additive:

$$U(\boldsymbol{R}, Z) = \int \mathrm{d}\boldsymbol{r} \int_{-\infty}^{+\infty} dz\, n(\boldsymbol{r}, z) V(|\boldsymbol{R} - \boldsymbol{r}|^2 + |Z - z|^2) \,. \tag{4.13}$$

Here $n(\boldsymbol{r}, z)$ is the liquid density at site $(\boldsymbol{r}, z)$. For an incompressible liquid with a sharp interface at $z = h(\boldsymbol{r})$, eq. (4.13) may be rewritten as

$$U(\boldsymbol{R}, Z) = n_{\mathrm{He}} \int \mathrm{d}\boldsymbol{r}\, W(|\boldsymbol{R} - \boldsymbol{r}|^2 + |Z - h(\boldsymbol{r})|^2) \,, \tag{4.14}$$

with $V \equiv -\partial W/\partial Z$. In view of the discussion of section 3.2 this ansatz is clearly very crude, but it suffices for our present purpose. Expanding $U(\boldsymbol{R}, Z)$ for small values of $h(\boldsymbol{r})$ leads with the normal mode decomposition eq. (4.1) to

$$U(\boldsymbol{R}, Z) = U_0^h(Z) - A^{-1/2} \sum_{\boldsymbol{q}} h_{\boldsymbol{q}}\, \mathrm{e}^{\mathrm{i}\boldsymbol{q}\cdot\boldsymbol{R}}\, \frac{\partial}{\partial Z} U_{\boldsymbol{q}}^h(Z) + \cdots \tag{4.15}$$

where

$$U_{\boldsymbol{q}}^h(Z) = \sum_{n=0}^{\infty} \frac{1}{n!} \left(\frac{1}{2A} \sum_{\boldsymbol{q}'} h_{\boldsymbol{q}'} h_{-\boldsymbol{q}'} \frac{\partial^2}{\partial Z^2} \right)^n U_{\boldsymbol{q}}(Z), \tag{4.16}$$

with

$$U_{\boldsymbol{q}}(Z) = n_{\mathrm{He}} \int \mathrm{d}\boldsymbol{r}\, \mathrm{e}^{\mathrm{i}\boldsymbol{q}\cdot\boldsymbol{r}} \int_{-\infty}^{0} \mathrm{d}z\, V(r^2 + (Z - z)^2). \tag{4.17}$$

To arrive at eq. (4.15) only those terms should be retained in the expansion that may contribute to zero- or one-ripplon matrix elements of (unperturbed) harmonic ripplons. The first term in the expansion eq. (4.15) relates to the static ($\boldsymbol{q} = 0$) adsorption potential, the second term gives the dynamical coupling to single ripplons. Thermally averaging $U_q^h(Z)$ yields:

$$\langle\langle U_{\boldsymbol{q}}^h(Z)\rangle\rangle = n_{\mathrm{He}} \int \mathrm{d}\boldsymbol{r}\, \mathrm{e}^{\mathrm{i}\boldsymbol{q}\cdot\boldsymbol{r}} \times \int_{-\infty}^{0} \mathrm{d}z\, V(r^2 + (Z - z)^2) \tfrac{1}{2} \mathrm{erfc}[z/(2\langle h^2\rangle)^{1/2}], \tag{4.18}$$

where $\langle h^2 \rangle$ is the rms surface fluctuation due to the ripplons, derived in section 4.1 For $\boldsymbol{q} = 0$, eq. (4.18) provides an improved approximation to the adsorption potential, accounting for the presence of ripplons. The complementary error function has the same origin as the Debye–Waller factor in neutron scattering. It replaces the sharp interface at $z = 0$ in eq. (4.17) and may be interpreted as the ripplon contribution to the density profile. Using $\langle h^2 \rangle = 1.6$ Å, as follows from eq. (4.11), one finds that for $T = 0$ K the density drops from 90% to 10% of the bulk density over a distance of 3.6 Å. Comparing this result with the 4.4 Å used by Mantz and Edwards (ME) shows that the ripplon contribution to the density profile is important. The dependence of eq. (4.18) on $\langle h^2 \rangle$ further implies with eq. (4.12) a temperature dependent adsorption energy. This effect should be small (in particular for helium films) as the width of the density profile is substantially smaller than the extent of the bound-state wavefunction.

To arrive at a better approximation to the adsorption potential one has to improve upon the above procedure by introducing pair correlations and include the phonon contribution to the surface profile. Authors interested in the atom surface scattering problem have bootstrapped themselves to this point by using a step-function profile and constructing an *effective* H He pair potential that reproduces the ME-adsorption potential on the level of eq. (4.17) (with $\boldsymbol{q} = 0$), while leaving out all terms in the expansion of $U(\boldsymbol{R}, Z)$ that lead to the Debye-Waller factor. Zimmermann and Berlinsky (ZB) used a Morse potential to approximate the ME-results. This form for the potential allows an accurate fit to the well region of the ME-potential and has the advantage of allowing analytic solution of the wavefunctions. Kagan and Shlyapnikov (KS) used the same approach, but accounted for the proper long-range behavior by adding a $-\alpha_3/Z^3$ van der Waals attractive tail. Relativistic retardation effects in the H–He interaction are very small and therefore neglected in all papers on the subject.

Currently, preference is given to a slightly different approach. It has been established that atom surface scattering, if at all sensitive to the adsorption potential, is sensitive to the value of the bound-state energy rather than to the detailed shape of the potential [69]. Therefore, the flexibility of the Morse form is better used to match the experimental adsorption energy of 1 K rather than to fit the ME-potential. For helium films the substrate may affect the van der Waals attractive tail. This effect can be included by adding to the potential a term $\sim (Z + d)^{-3}$ that accounts for the replacement of bulk helium by a substrate, leaving a film of the desired thickness d. At this level retardation effects due to the substrate have to be included. A recent choice for an effective surface adsorption potential

including all these effects is given by Hijmans et al. [70]:

$$U_0(Z) = U_m(Z) - f(Z)\alpha_3 Z^{-3} - g(Z)C_s\alpha_3(Z+d)^{-3}, \tag{4.19}$$

where $\alpha_3 = 219.7$ K Å^3 is the van der Waals coefficient for H on bulk ^{4}He and

$$U_m(Z) = U_{min}\left[e^{-2\beta(Z-Z_0)} - 2\ e^{-\beta(Z-Z_0)}\right] \tag{4.20}$$

is the Morse potential, with $U_{min} = 5.14$ K, $\beta = 0.52$ Å^{-1} and $Z_0 = 4.2$ Å, while $f(Z)$ and $g(Z)$ are cross-over functions defined by

$$f(Z) = \tfrac{1}{2}\tanh[\beta(Z - Z_c)] + \tfrac{1}{2}, \tag{4.21}$$

$$g(Z) = \left[d_0 - (d_0 + d + Z)\ e^{-2(Z+d)/d_0}\right](Z+d)^{-1}. \tag{4.22}$$

Here $Z_c = 13$ Å is the Morse-van der Waals cross-over point and d_0 the retardation length, which depends on the substrate. C_s is a numerical constant such that C_s+1 represents the ratio of the van der Waals attraction of the H-atom due to the substrate and a bulk helium underlayer.

4.3. Surface adsorption: sticking coefficient

The first and most important scattering process to describe is surface adsorption or sticking. This process includes all scattering channels in which atoms end up in a surface-bound state. The term sticking is somewhat misleading as the atoms are in fact highly mobile in the adsorbed state, see eq. (3.18), and desorb after a short residency time.

Some characteristic features of the sticking channel follow directly from the conservation laws. In the low-energy limit, i.e., for incident energies $E \ll \varepsilon_a$, the energy liberated in the adsorption, ε_a, has to be shared between the adsorbed atom and an excitation in such a way that atom and excitation have equal and opposite momentum, $\pm\hbar\boldsymbol{q}_a$, along the surface. For ripplons on bulk helium this implies $\hbar^2 q_a^2/2m + \hbar\omega_{q_a} = \varepsilon_a$ and a corresponding wavelength $\lambda_a \equiv 2\pi/q_a \approx 48$ Å. For phonons the situation is slightly different. Where in the ripplon case the energy is more or less equally shared between ripplon and adsorbed atom, in phonon mediated adsorption more than 90% of ε_a is transferred to the excitation, $q_a \approx \varepsilon_a/\hbar u$, or $\lambda_a \approx 95$ Å. Both the ripplon and phonon wavelengths mentioned above are substantially smaller than the wavelength of the corresponding thermal excitations: 95 Å for ripplons and 571 Å for phonons at $T = 200$ mK.

Hence, adsorption processes stimulated by thermal excitations may be ruled out for typical experimental conditions ($T \lesssim 0.5$ K).

4.3.1. Ripplon mediated adsorption

The sticking probability of H on ^{4}He was first calculated by Zimmermann and Berlinsky (ZB) [71] and by Kagan and Shlyapnikov (KS) [72, 74] within first-order time dependent perturbation theory. Writing the wavefunction as a simple product in the notation of eq. (3.17), the transition rate to surface bound states under creation or annihilation of a single ripplon is

$$\Gamma_s(\varepsilon) = \frac{2\pi}{\hbar}\frac{1}{A}\sum_{\boldsymbol{q}}\frac{\hbar q \tanh(qd)}{2\rho_0\omega_q}\left|\langle B|\frac{\partial U_q(Z)}{\partial Z}|\sigma\rangle\right|^2 \times\left[(1+\bar{n}_{\boldsymbol{q}})\delta(E'+\hbar\omega_q - E) + \bar{n}_{\boldsymbol{q}}\delta(E'-\hbar\omega_q - E)\right]. \tag{4.23}$$

Here E and E' are the initial and final state energies of the adsorbing H-atom, respectively. For atoms incident at an angle θ with respect to the surface normal $\varepsilon \equiv E\cos^2\theta \equiv \hbar^2\sigma^2/2m$ is the energy associated with the normal motion at incidence; $\hbar\omega_q$ is the energy of the ripplon excited or annihilated. The bound state is normalized to unity. By normalizing the initial-state wavefunction to unit incident flux eq. (4.23) represents the sticking probability. For large Z the asymptotic form of the initial state is given by

$$\phi(Z) = 2(m/\hbar\sigma)^{1/2}\sin[\sigma Z + \delta(\sigma)] \tag{4.24}$$

where δ is a phase shift. The potential $U_q(Z)$ is given by eq. (4.17), where the effective pair potential V is chosen such that $U_0(Z)$ reproduces the desired static adsorption potential.

In the low-energy limit and for films of thickness $d \gg \lambda_a$ only the terms with $q \approx q_a$ will contribute to the sum in eq. (4.23). With eq. (4.6) the thermal contributions are calculated to be negligibly small: $\bar{n}_{\boldsymbol{q}_a} \approx 0.06$ for a wall temperature $T_w = 200$ mK. With these approximations eq. (4.23) reduces to

$$s(\varepsilon) \approx \tfrac{1}{2}\frac{(q_a/\gamma\rho_0)^{1/2}}{\hbar^2 q_a/m + \frac{3}{2}\hbar(\gamma q_a/\rho_0)^{1/2}}|\langle B|(\frac{\partial U_{q_a}(Z)}{\partial Z}|\sigma\rangle|^2. \tag{4.25}$$

The only ε energy dependence in this equation appears through the σ-dependence of the initial-state wavefunction. To illustrate this point in

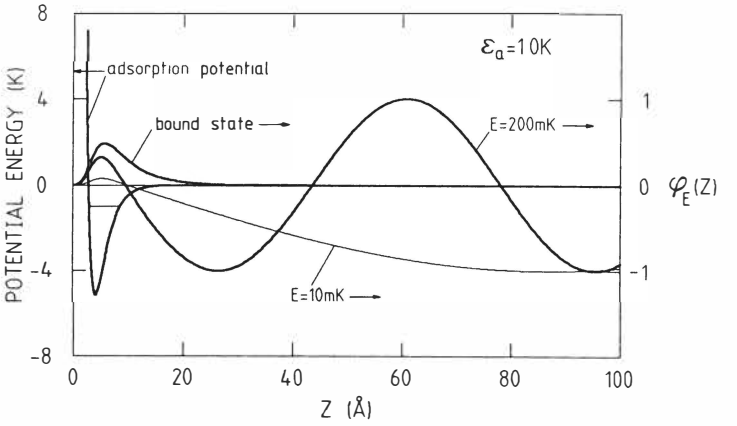

Fig. 9. Surface adsorption potential of H on ^{4}He and corresponding eigenstates. Apart from the bound-state wavefunction two continuum states are shown with normal energies 10 and 200 mK.

fig. 9 two continuum wavefunctions with different normal energies are shown. The wall temperature does not appear as the surface is effectively in its ground state. It was shown by ZB and KS that for vanishingly low incident energies, the matrix element scales as $E^{1/2}\cos\theta$ so that for a thermal ensemble of atoms at temperature T_g, $s \sim T_g^{1/2}$. This limit is known as the quantum reflection regime. Goldman [75] numerically investigated the influence of the detailed potential shape. He pointed out that depending on the choice of the van der Waals coefficient α_3, the value of s may vary by orders of magnitude and is always larger than the result of ZB, who neglected the long-range tail altogether. He found that in extreme cases the low-energy limit may only be reached for temperature below 1 μK. The importance of the long-range behavior of surface potentials for the quantum reflection regime was also stressed by Brenig and collaborators in a more general context [76]. Goldman also varied the repulsive core of the potential, while fixing ε_a, but this turned out to have little effect on the limiting behavior of s.

The recent results of Hijmans et al. for the low-energy limit of sticking are shown in fig. 10. These results were obtained with eq. (4.25). The matrix element was numerically evaluated using the HWS-potential eq. (4.19).

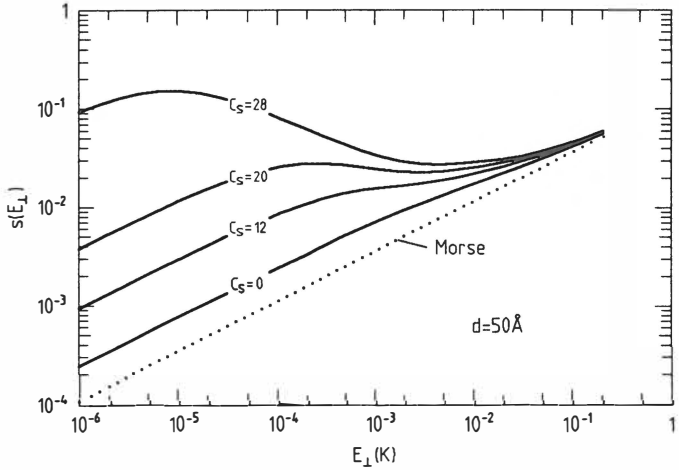

Fig. 10. The sticking coefficient at normal incidence as calculated by Hijmans et al. [70]. For a discussion of the various curves see text.

The dotted curve corresponds to the Morse potential and is described by

$$s(E,\theta) = s_0^{\mathrm{r}} \left(\frac{E}{\varepsilon_{\mathrm{a}}}\right)^{1/2} \cos\theta, \tag{4.26}$$

with $s_0^{\mathrm{r}} \approx 0.11$. An analytic expression in terms of the Morse potential parameters is given by ZB. The solid curves in fig. 10 correspond to a helium film of 50 Å thickness and for various retarded substrate potentials. The value of s increases with C_{s}. The curve with $C_{\mathrm{s}} = 0$ corresponds to bulk helium. The dashed curves correspond to the same series of substrates, but leaving out the retardation.

4.3.2. Phonon-mediated adsorption

From a practical point of view, the phonon contribution to the sticking process is unimportant. This was demonstrated by KS in their first paper on the subject [72]. Nevertheless it seems appropriate in the present context to spend a few words on this process. Surely there is no a priori reason to disregard the phonons. Leaving out thermally stimulated processes from the onset and choosing the normalization convention of the

previous section, the sticking probability is written as

$$s(\varepsilon) = \frac{2\pi}{\hbar}\frac{1}{V}\sum_{\boldsymbol{q}}\frac{\hbar q^2}{2\rho_0\omega_q}|\langle B|U_q(Z)|\sigma\rangle|^2\delta(E' + \hbar\omega_q - E)\,. \tag{4.27}$$

Only phonons with $q \approx q_{\mathrm{a}}$ will contribute in the low-energy limit. Using the phonon dispersion $\omega_q = uq$, where $u \approx 239$ m/s is the speed of sound in ^{4}He, and after integrating-out the delta-function one finds for bulk helium

$$s(E,\theta) = \frac{1}{2\pi\hbar}\frac{q_{\mathrm{a}}^3}{\rho_0 u^2}|\langle B|U_{q_{\mathrm{a}}}(Z)|\sigma\rangle|^2\ . \tag{4.28}$$

In complete analogy with the ripplon mediated case all dependence on ε enters through the σ-dependence of the initial-state wavefunction. This results in the same ε-dependence of ripplon and phonon channels in the low-energy limit. For a Morse potential the matrix element is $\hbar U_{\min}(E/\varepsilon_{\mathrm{a}})^{1/2} \times \cos\theta$ so that [72]

$$s(E,\theta) = s_0^{\mathrm{ph}}\left(\frac{E}{\varepsilon_{\mathrm{a}}}\right)^{1/2}\cos\theta, \tag{4.29}$$

with $s_0^{\mathrm{ph}} \equiv (U_{\min}/2\pi)(q_{\mathrm{a}}^3/\rho_0 u^2) \approx 4 \times 10^{-4}$. Comparing with eq. (4.26) one finds that the atoms couple much stronger to the ripplons than to the phonons, meaning that the latter coupling may be neglected.

4.3.3. Adsorption near the saturation density

At surface densities within a factor 2 from the saturation density the physics of the adsorption process changes markedly as collective effects start to be important. This case was studied by Kagan et al. [73]. The effective adsorption energy is reduced by the interatomic interactions in the adsorbate. The leading adsorption mechanism is stimulated capture into the quasi-condensate of the adsorbed gas. Two temperature regimes may be distinguished. For $T > 0.1$ K the process turns out to be assisted by bulk phonons. For $T < 0.1$ K the process can be ripplon assisted, but only if (re)desorption of particles from the quasi-condensate may be avoided.

4.4. Thermal averaging, detailed balance and thermal desorption

Before continuing the discussion of individual scattering channels we have a look at some simple expressions for thermal averages of atomic flux re-

lated probabilities, such as the sticking probability. The discussion will be restricted to probabilities $W(E,\theta)$ that may be expressed in the form

$$W(E,\theta) = W_0 E^n \cos^m \theta\,, \tag{4.30}$$

where E is the kinetic energy of atoms incident at angle θ with respect to the surface normal. The functional form of eq. (4.30) is chosen because it is typical for the limiting cases of atom surface scattering that are discussed in these lectures.

For a Boltzmann gas of density n_g and temperature T the distribution of the flux incident on a surface area A may be expressed as $\Phi_{in}(E,\theta;T) = \Phi P_B(E,\theta;T)$, where $\Phi = \frac{1}{4} n_g \bar{v} A$ is the total flux and

$$P_B(E,\theta;T) \equiv (E/\pi {k_B}^2 T^2) \exp(-E/k_B T) \cos\theta \sin\theta \tag{4.31}$$

is the normalized thermal *flux* distribution. As the transition probabilities are defined as transition rates per unit incident flux, thermal averaging is properly done with the distribution eq. (4.31). For eq. (4.30) this yields

$$W(T) = W_0 \Gamma(n+2) \frac{2(k_B T)^n}{m+2}\,, \tag{4.32}$$

where $\Gamma(z)$ is the gamma function. By leaving out the θ-integration in the averaging, the gas average eq. (4.32) may be related to a beam average for a thermal beam incident at angle θ:

$$W(T,\theta) = \tfrac{1}{2}(m+2) W(T) \cos^m \theta\,. \tag{4.33}$$

Equations (4.30), (4.32) and (4.33) may serve to conveniently interrelate various expressions for transition probabilities presented in this text and in the literature. At the same time it should be emphasized that special care is required in cases where grazing incidence is important and eq. (4.30) tends to break down.

To derive the flux distribution $\Phi_{out}(E,\theta;T)$ for the atoms desorbing from the surface detailed balance should be enforced. At equilibrium:

$$S(T)\Phi_{out}(E',\theta';T) = S(E,\theta)\Phi P_B(E,\theta;T)\,. \tag{4.34}$$

Here $\Phi_{out}(E,\theta;T)$ is normalized to the *total* incident flux. Notice that eq. (4.34) has this particularly simple form because the atoms fully thermalize in the adsorbed state. Combining eqs. (4.26), (4.32) and (4.34) one

finds for the desorption channel at low temperature

$$\Phi_{\text{out}}(E', \theta'; T) = (\Phi/k_{\text{B}}T)(E/\pi k_{\text{B}}T)^{3/2} \exp(-E/k_{\text{B}}T) \cos^2\theta \sin\theta \,. \tag{4.35}$$

In view of the full thermalization on the surface, this expression should remain valid also for a non-thermal incident flux.

4.5. Direct inelastic scattering

Apart from scattering into a surface bound state, H-atoms may also exchange energy with ripplons in direct scattering processes, i.e., in collisions without adsorption. Direct processes differ importantly from sticking as in the absence of adsorption the energetics exclusively involve thermal energies. Hence ripplons of very low $\boldsymbol{q}$-values may be excited and the quasi-classical approximation, eq. (4.7), holds. Interestingly enough for $\boldsymbol{q} \to 0$ direct processes are independent of the adsorption potential. This was pointed out by Tiesinga et al. [77]. All put together, for H-atoms with de Broglie wavelength much shorter than the wavelengths of thermal ripplons, the picture emerges of classical particles colliding with the fluctuating surface of a classical incompressible liquid. This is exactly the approximation made by Castaing and Papoular to calculate the contribution of direct scattering to the Kapitza resistance of the H He interface [78]. The argument also provides plausibility to the remarkably good agreement between the results with this classical approach and those of subsequent fully quantum mechanical calculations, such as those by Statt or Goldman [79, 75].

To further outline the essential features of direct scattering we remain within the perturbative approach of the previous sections, writing the probability for direct scattering under emission or absorption of a ripplon as

$$W_{\text{d}}(\varepsilon) = \frac{L}{\pi} \int \mathrm{d}\sigma' \int \mathrm{d}q \, \frac{q^2 \tanh(qd)}{2\rho_0\omega_q} |M(\sigma', \sigma; q)|^2 \times \left[(\bar{n}_{\boldsymbol{q}} + 1)\delta(E' + \hbar\omega_q - E) + \bar{n}_{\boldsymbol{q}}\delta(E' - \hbar\omega_q - E)\right] . \tag{4.36}$$

The initial-state wavefunction is normalized to unit incident flux as in eq. (4.24) and the final state $\phi'(Z)$ is normalized to unity in a box of length L. Its asymptotic form for large Z is

$$\phi'(Z) = (2/L)^{1/2} \sin[\sigma' Z + \delta(\sigma')] \,. \tag{4.37}$$

The matrix element is given by

$$M(\sigma', \sigma; q) = \lim_{z_0 \to \infty} \int_{-z_0}^{+z_0} \mathrm{d}Z \, \phi'(Z) \frac{\partial U_q(Z)}{\partial Z} \phi(Z) \,, \tag{4.38}$$

where the limit should be taken while maintaining $z_0 < L$. The dependence of eq. (4.36) on ε and on the wall temperature appears through $\bar{n}_{\boldsymbol{q}} \approx k_{\mathrm{B}} T_{\mathrm{w}} / \hbar \omega_q$, while the energy of the scattering atom enters through the σ-dependence of the initial and final states. At this point we distinguish two interesting limiting regimes: the quasi-elastic regime and the low-energy limit.

4.5.1. Quasi-elastic scattering ($E \gg k_{\mathrm{B}} T_{\mathrm{w}}$)

For fast atoms incident on a cold helium surface, direct inelastic scattering is quasi-elastic, i.e., the momentum transfer and hence the scattering angle θ' are small, $\theta' \approx \tan \theta' = q/\sigma \ll 1$, while $\sigma' \approx \sigma$. To illustrate this point note that a 0.2 K atom at normal incidence will be scattered over $\theta_T \approx 22\,^\circ$ by a 0.2 K thermal ripplon and over $0.6\,^\circ$ by the cross-over ripplon.

Ripplon emission and absorption are equally important. Hijmans and Shlyapnikov [80] show explicitly by partial integration of eq. (4.38) that for $q \to 0$ the matrix element is independent of the potential and may be expressed in analytical form as

$$\lim_{q \to 0} M(\sigma, \sigma; q) = - \left(\frac{8m}{\hbar \sigma L} \right)^{1/2} \varepsilon \,. \tag{4.39}$$

After removal of the delta function in eq. (4.36) by integration over σ' and transforming the q-integration into a θ'-integration we have

$$W(\varepsilon, \theta'_{\max}) = w_0 T_{\mathrm{w}} \varepsilon \ln[1 + (\theta'_{\max}/\theta'_0)^2], \tag{4.40}$$

where $w_0 \equiv (2m{k_{\mathrm{B}}}^2/\pi\gamma\hbar^2) = 0.1 \ \mathrm{K}^{-2}$, with θ'_0 the average scattering angle induced by a ripplon of cross-over wavelength λ_0. For $T_{\mathrm{g}} = 0.2$ K and a helium film of 100 Å thickness $\bar{\theta}'_0 \approx 0.6\,^\circ$. For a thermal beam at normal incidence characterized by a temperature T_{g}, the probability for quasi-elastic scattering within a scattering angle $\theta'_{\max}$ is

$$W_{\mathrm{d}}(\theta'_{\max}) \approx \frac{4m}{\pi\gamma} \left(\frac{k_{\mathrm{B}}}{\hbar} \right)^2 T_{\mathrm{w}} T_{\mathrm{g}} \ln \left[1 + \left(\frac{\theta'_{\max}}{\bar{\theta}'_0} \right)^2 \right] \tag{4.41}$$

In view of the weak dependence on the scattering angle this expression

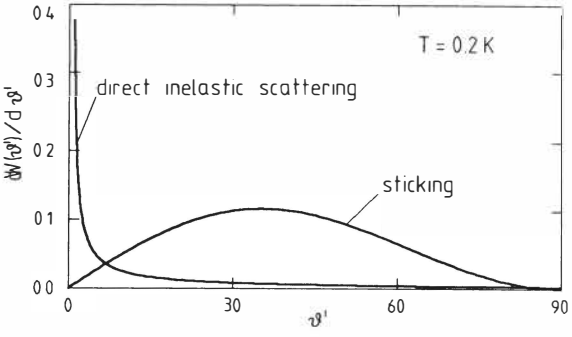

Fig. 11. Differential scattering probability at normal incidence $(dW(\theta')/d\theta')$ as a function of scattering angle θ'. Note the dominance of small scattering angles for direct processes.

remains approximately correct for $T_g \approx T_w$. To illustrate the concept of quasi-elastic scattering the derivative of eq. (4.41) with respect to θ'_{max} is shown in fig. 11.

4.5.2. Low-energy scattering limit $(E \ll k_B T_w)$

Another interesting case of direct inelastic scattering is the case where very cold atoms scatter from a relatively warm, i.e., thermally activated helium surface. Due to momentum conservation in this case the atoms will scatter off with the ripplon momentum q parallel to the surface. As the atom also has to carry off the ripplon energy $\hbar\omega_q$, the atoms leave the surface at some angle θ_d with the surface normal, which is independent of the incident energy. One immediately shows, using the dispersion relation, that for helium films at temperatures such that $\lambda_T \ll \lambda_0$, this departure angle is also independent of surface temperature:

$$\tan\theta_d = \left[\frac{2m}{\hbar}\left(\frac{\gamma d}{\rho_0}\right)^{1/2} - 1\right]. \tag{4.42}$$

For a film thickness $d \approx 100$ Å one calculates $\theta_d = 45°$. The departure angle is an important signature of the process discussed here. At sufficiently low temperatures, $T_w \lesssim 100$ mK, the matrix element becomes

$$\lim_{q\to 0} M(\sigma', \sigma; q) = -\left(\frac{8m}{\hbar\sigma L}\right)^{1/2} (\varepsilon'\varepsilon)^{1/2}, \tag{4.43}$$

independent of the adsorption potential. The average transition probability for a thermal beam at normal incidence is

$$W_{\mathrm{d}} \approx \pi^{-1/2} \frac{2m}{\gamma} \left(\frac{k_{\mathrm{B}}}{\hbar} \right)^2 T_{\mathrm{w}}^{3/2} T_{\mathrm{g}}^{1/2} . \tag{4.44}$$

Notice that eq. (4.44) has the same low-temperature limit as the sticking process. Numerical evaluation shows that the probability for direct inelastic scattering is many orders of magnitude smaller than the sticking probability.

4.6. Thermal accommodation and boundary resistance

As is well known, at low temperatures thermal contact across interfaces becomes very poor. For non-conducting materials this arises from Kapitza-type thermal boundary resistances. It follows from the previous sections that the interface between H gas and liquid helium is no exception to this rule, although it compares favorably with the usual acoustic mismatch. Any inelastic scattering process will contribute to the heat transfer. To quantify the quality of thermal contact, the present section is devoted to relating the scattering probabilities derived in the previous sections to thermal accommodation.

The heat transfer is characterized by the thermal accommodation coefficient α. If the energy carried by an incident flux of atoms is fully accommodated ($\alpha = 1$) the atoms leave the surface at wall temperature. In the absence of any accommodation ($\alpha = 0$) no energy is exchanged. The accommodation coefficient is defined as

$$\alpha = \lim_{T_{\mathrm{g}} \to T_{\mathrm{w}}} \frac{\dot{Q}_{\mathrm{g}} - \dot{Q}_{\mathrm{o}}}{\dot{Q}_{\mathrm{g}} - \dot{Q}_{\mathrm{w}}} , \tag{4.45}$$

where $\dot{Q}_{\mathrm{g}}$, $\dot{Q}_{\mathrm{o}}$ and $\dot{Q}_{\mathrm{w}}$ represent, respectively, the average energy fluxes carried by the incident flux Φ_{in}, the actual outgoing flux Φ_{out} and a fully accommodated outgoing flux. In steady state $\Phi_{\mathrm{out}} = \Phi_{\mathrm{in}} \equiv \Phi = \frac{1}{4} n_{\mathrm{g}} \bar{v} A$ and, accounting only for kinetic energy, one has

$$\dot{Q}_{\mathrm{g}} = 2 k_{\mathrm{B}} T_{\mathrm{g}} \Phi ; \qquad \dot{Q}_{\mathrm{w}} = 2 k_{\mathrm{B}} T_{\mathrm{w}} \Phi . \tag{4.46}$$

The heat flux $\dot{Q}_{\mathrm{o}}$ is related to the net heat flux $\dot{Q}$ from gas to surface by the relation $\dot{Q}_{\mathrm{o}} = \dot{Q}_{\mathrm{g}} - \dot{Q}$. Thus for $T_{\mathrm{g}} \to T_{\mathrm{w}}$, $\dot{Q}$ may be expressed as

$$\dot{Q} = \alpha \Phi 2 k_{\mathrm{B}} (T_{\mathrm{g}} - T_{\mathrm{w}}) . \tag{4.47}$$

Comparing eq. (4.47) with the usual definition of the Kapitza resistance, $R_K = \lim_{\Delta T \to 0} \Delta T/\dot{Q}$, one finds

$$R_K^{-1} = 2\alpha k_B \Phi . \tag{4.48}$$

An important expression, due to Goldman [75], relates the accommodation coefficient for the sticking process to the thermally averaged sticking coefficient in steady-state. To derive this relation assume that s depends on T_g and T_w in a separable manner $s(T_g, T_w) \equiv f(T_w)S(T_g)$. Then, the net heat transfer is

$$\dot{Q} = -f(T_w)\{S(T_g) \int \Phi_{out}(E, \theta; T_w) E \, dE \, d\theta - \int S(E, \theta) \Phi P_B(E, \theta; T_g) E \, dE \, d\theta\} , \tag{4.49}$$

where $\Phi_{out}(E, \theta; T)$ represents the distribution function of the flux of atoms leaving the surface, normalized to the incident flux. Note that Φ_{out} depends only on T_w as the atoms fully thermalize after adsorption. The detailed balance condition for thermal equilibrium may be used to eliminate the unknown distribution Φ_{out} from eq. (4.49). An expression for α follows by substitution of the result into eq. (4.45) and evaluating the limit $T_g \to T_w$ for a Boltzmann gas

$$\alpha(T) = \tfrac{1}{2} s(T) \int S(E, \theta) \frac{\partial}{\partial T} \left[\frac{P_B(E, \theta; T)}{k_B S(T)} \right] E \, dE \, d\theta . \tag{4.50}$$

Straightforward evaluation of the integral results in

$$\alpha(T) = s(T) \left[1 + \frac{1}{2} \frac{d \ln S(T)}{d \ln T} + \frac{1}{2} \frac{d^2 \ln S(T)}{(d \ln T)^2} \right] \tag{4.51}$$

This expression is equivalent to the expression of Goldman if the explicit dependence on T_w is suppressed, i.e., for $s(T) = S(T)$.

5. Experimental results

5.1. Measurements of the sticking coefficient

5.1.1. Magnetic resonance experiments

The sticking coefficient was first measured by Jochemsen et al. [81, 3] at UBC with magnetic resonance on H at 1420 MHz using pure ^{4}He and pure

^{3}He surface coverages. The resonance signal shows a frequency shift $\Delta\omega$ and a decay rate T_2^{-1} that depend on the surface adsorption. For an atom resident on the surface the resonance frequency is shifted by an amount Δ_s, leading to an average phase shift per sticking event $\phi = 2\pi\tau_a\Delta_s$ where τ_a is the average residency time on the surface given in eq. (3.2). The phase shift ϕ depends exponentially on temperature. If both the distribution of the residency times and that of times between sticking events obey Poisson statistics, the frequency shift and decay rate may be given by [81]

$$\Delta\omega = \frac{1}{\tau_b}\frac{\phi}{1+\phi^2}, \tag{5.1}$$

$$\frac{1}{T_2} = \frac{1}{\tau_b}\frac{\phi^2}{1+\phi^2}, \tag{5.2}$$

where τ_b is the average time between sticking events. Equations (5.1) and (5.2) imply a maximum frequency shift $\Delta\omega_{max} = (2\tau_b)^{-1}$ and a maximum decay rate $(T_2^{-1})_{max} = \tau_b^{-1}$, which may be found by varying the temperature. The authors determined the sticking coefficient s by comparing the calculated (by computer simulation) mean time between wall-collisions τ_c to the observed mean time between sticking events τ_b, assuming $\tau_c/\tau_b = s(T)$. This is only approximately correct as will be discussed in section 5.3 Jochemsen et al. found $s = 0.016(5)$ for H on ^{3}He at $T \approx 95$ mK and $s = 0.035(4)$ for H on ^{4}He at $T \approx 200$ mK. A reanalysis by Morrow and Hardy [82] resulted in a value of $s = 0.046$ for H on ^{4}He. The results are shown in fig. 12.

5.1.2. Capillary flow experiment

Berkhout et al. [83] used a capillary flow method to extract the sticking coefficient. In this experiment a buffer volume V is filled with H to a density n_g. The gas was then allowed to flow through a capillary to a volume kept free of H-atoms. Under these conditions $T_g = T_s$. The flow Φ through the capillary depends on the H flux entering the capillary and the transmission coefficient (Clausing factor) K:

$$\Phi = \tfrac{1}{4}n_g\bar{v}AK \equiv N/\tau, \tag{5.3}$$

where N is the number of atoms in the buffer volume, and A the entrance orifice of the capillary. By measuring τ the Clausing factor follows from $K = \tau_0/\tau$, where $\tau_0^{-1} \equiv \frac{1}{4}\bar{v}A/V$. To determine s the relation between K and s must be known. In the Knudsen flow regime and for $s = 1$ the Clausing factor assumes its Knudsen value K_K, purely determined by

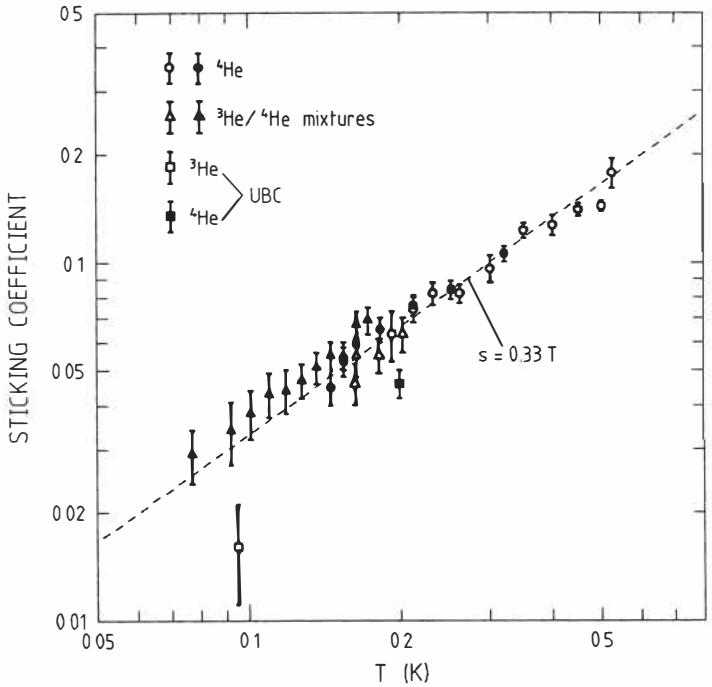

Fig. 12. The sticking probability as determined by Berkhout et al. [83] with the capillary method. Also the UBC results [82] are shown.

geometrical factors and thus temperature independent. For capillaries with large ratio of length l over radius a, $K_K = 8a/3l$. In the geometry of Berkhout et al. $K_K = 0.0284$ [83]. For $s = 0$ the Clausing factor is 1, that is, every particle entering the capillary will scatter specularly until it leaves at the other end. The relation between s and K for several values of interest of s was determined by a one-speed Monte Carlo computer simulation. This is only approximately correct. We return to this point in the discussion. The capillary flow results are given in fig. 12. The sticking coefficient turns out to be proportional to T and may be given within 10% experimental accuracy as $sT^{-1} = 0.33\ \mathrm{K}^{-1}$ in the range $73 < T < 526$ mK. The results are shown in fig. 12. It is remarkable that within experimental error s is the same for ^{4}He surfaces and for surfaces of ^{3}He ^{4}He mixtures. The surface of these mixture films is believed to be very similar to that of pure ^{3}He films [84].

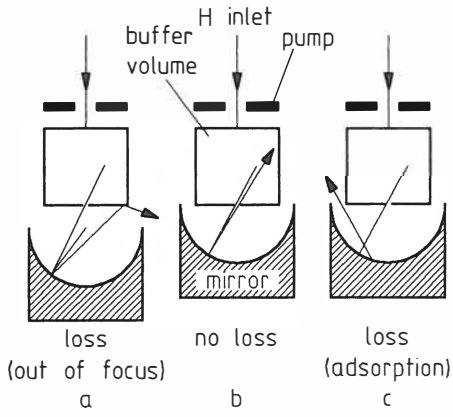

Fig. 13. The principle of the mirror experiment. For a discussion see the text.

5.1.3. Mirror experiment

To demonstrate the dominance of elastic scattering Berkhout et al. [85] measured the specular reflectivity of a helium surface at normal incidence with a helium coated hemispheric mirror. This experiment is quite similar in concept to the capillary flow experiment described before. A buffer volume V_B is filled with hydrogen to a density of 10^{14} atoms/cm^3. The gas expands through an orifice and is detected on a pumping plate H-flux detector [86] which also keeps the secondary volume free of hydrogen. The exponential decay time of the flux escaping the buffer volume is measured. If specular reflection is dominant this quantity should depend strongly on the position of the hemispheric mirror as illustrated in fig. 13. If the center of the mirror does not coincide with the exit orifice of the buffer volume V_B, as sketched in fig. 13a, the buffer volume will be emptied as in the absence of the mirror. However, if mirror-center and exit-orifice coincide, as shown in fig. 13b, the beam of atoms expanding through the diaphragm is reflected back into the buffer volume, causing the exponential decay time to be much longer. Under these conditions, the loss from the storage volume depends on the reflectivity of the mirror, which in turn depends on the inelastic scattering phenomena at the helium surface (see fig. 13a). If the dimensions and temperature of the cell are accurately known, one may calculate the loss factor χ representing the probability that an atom is *not* scattered back into the buffer volume

$$\chi \equiv \frac{\tau_0}{\tau} \approx -\frac{\tau_0}{N}\frac{\mathrm{d}N}{\mathrm{d}t} \,. \tag{5.4}$$

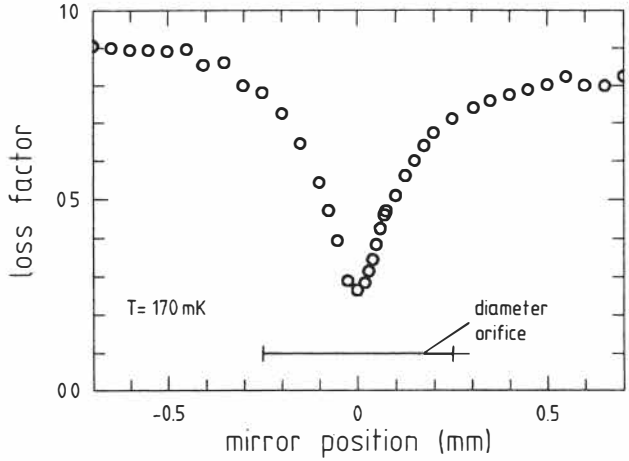

Fig. 14. The loss factor as a function of the vertical mirror position as observed by Berkhout et al. [85].

Here N is the total number of atoms in the buffer volume and $\tau_0 \equiv 4V_B/\bar{v}A$ the first-order decay time in the absence of the mirror and A is the cross-sectional area of the orifice. In fig. 14 the loss factor is shown as a function of the position of the mirror. With the mirror far from focusing conditions the loss is found to approach unity as in the absence of the mirror. As seen from the figure, the loss from the buffer volume may be reduced by a factor 4–5 by proper adjustment of the mirror. This represents the first demonstration of focusing of an atomic beam by means of a mirror. In the absence of lateral misalignment and mirror aberrations the loss at the minimum of the position scan corresponds to the deviation from perfect reflectivity of the mirror. In this way specular reflectivities larger 80% were observed. By measuring the reflectivity as a function of temperature and comparing with the capillary flow data some evidence for the occurrence of quasi-elastic scattering was obtained in these experiments.

5.2. Measurements of the accommodation coefficient

To measure the accommodation coefficient of H on ^{4}He, several experimental methods have been used. The results are compiled in fig. 15. In the first experiment, by Salonen et al. [87] ballistic heat transport was measured with a time-of-flight method. A pulsed heater was used to increase

the temperature of a helium film. H-atoms striking this film will on average gain some kinetic energy. This increase in kinetic energy was observed as a net heat transfer to a bolometer positioned opposite to the heater. At ambient temperatures of about 400 mK, in addition a signal with a slower time-of-flight response due to evaporating He atoms was observed. By subtracting signals with and without H in the sample cell the signal due to the H itself was obtained. From the comparison of this signal with the He signal, knowing the sticking coefficient for ^{4}He atoms incident on liquid ^{4}He surfaces to be very close to 1, the accommodation coefficient for H was obtained. The result was given as $\alpha = 0.2(1)$ in the temperature range 200 to 500 mK. Some indication of decreasing α with decreasing atomic speed was observed, but the signal-to-noise ratio did not allow any definite statement.

The heat loss of an electrically heated bolometer suspended in H gas by thin wires was measured by Salonen et al. [88]. The accommodation coefficient is found by applying eq. (4.45). A difficulty of this method is the determination of the gas temperature T_g of the atoms incident on the bolometer. For a small bolometer T_g approaches the ambient temperature in the limit that the mean free path goes to infinity. The measurements were made as a function of H density and extrapolated to zero density for several ambient temperatures but constant bolometer surface temperature. By extrapolating to zero temperature difference a value of $\alpha = 0.18(5)$ at 440 mK may be obtained. The authors saw evidence for an increasing accommodation coefficient with decreasing kinetic energy of the incident atoms.

An estimate for the accommodation coefficient was also reported by Bell et al. [89]. In this experiment the main objective was the measurement of relaxation and recombination of a sample of compressed H. The temperature difference was measured between both sides of a pancake-like sample bounded by a thermally floating and a rigidly pinned surface. The accommodation coefficient was obtained from a model involving heating due to surface and volume recombination, the thermal conductivity of the gas, the accommodation process itself and the Kapitza resistance of the liquid–solid interface. The authors extracted an accommodation coefficient varying from 0.8(4) at 600 mK down to 0.4(2) at 275 mK.

The most complete determination of α was done by Helffrich et al. [90], who used a method similar to that of Salonen et al. [88], but using lower H densities and a better characterized bolometer. The authors present a thorough analysis of the possible systematic errors inherent to this measurement method. The results are shown in fig. 15. The accommodation coefficient was found to be proportional to T and may be given within about 10% ex-

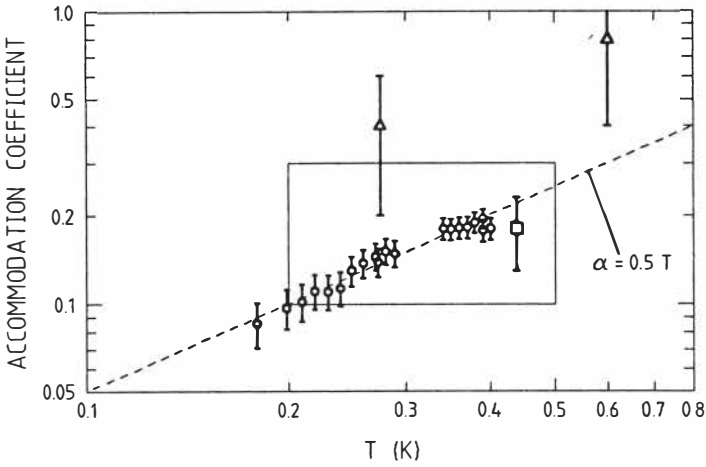

Fig. 15. Experimental results for the accommodation coefficient. Big rectangle ref. [87]; solid square ref. [88]; triangles ref. [89]; open circles ref. [90].

perimental accuracy as $\alpha T^{-1} = 0.5\ \mathrm{K}^{-1}$ in the range $180 < T < 400$ mK.

5.3. Discussion, recent developments and prospects

In evaluating and comparing the various experimental results for sticking and accommodation it may be useful to mention some limitations on their validity and use. The procedure used by the UBC group to extract the sticking coefficient from the magnetic resonance data has some clear limits to its validity [85]. As specular reflection and direct-inelastic scattering are (quasi) elastic processes, the speed of the H-atoms is conserved between sticking events, and the relation $\tau_c/\tau_b = s(T)$ is not valid. For perfectly rough walls, where the angle of incidence and reflection with respect to the macroscopic plane of the surface are uncorrelated, the correct relation is $\tau_b(v) = \tau_c(v)/s(v)$ with $\tau_c(v) = \tau_c\bar{v}/v$. The thermally averaged value for τ_b, which is observed, is found from

$$\tau_b = \int \tau_b(v)\Phi(v)\,\mathrm{d}v \Big/ \int \Phi(v)\,\mathrm{d}v, \tag{5.5}$$

in which $\Phi(v)$ is the incident flux on the surface. It is easy to show $s(v)$ should equal $mv^2/4k_BT_0$ if s is to have a linear temperature dependence $s = T/T_0$. With eq. (5.5) this results in $\tau_b = 4\tau_c/s(T)$. Similarly, for $s(T) \sim T^{1/2}$ the result is $\tau_b = 1.5\tau_c/s(T)$. Therefore, the exact relation

between s and τ_c/τ_b depends on the functional behavior of $s(v)$ and, if the walls are not perfectly rough, also on the geometry of the sample volume. Smooth walls tend to increase τ_b for a given value of s and τ_c. This means that the results of the UBC group are lower limits on the sticking coefficient.

Also the capillary flow data, analyzed with a one-speed simulation model may easily be criticized. A proper model should include a thermal average of $s(E,\theta)$ and as such requires input of energies outside the measured range of temperatures. The error made by the one-speed model is thus dependent on the temperature dependence extracted. An analysis of these errors is currently not available, but unpublished recent estimates show that these may be substantial for a linear temperature dependence [91]. In this respect the measurements of the accommodation appear to be cleaner.

It is also interesting to mention briefly the very recent results of Doyle et al. [92] who used ultra-cold H-atoms from a magnetic trap to measure s at much lower temperatures than in previous experiments. In these experiments $T_g \ll T_w$ and in view of the discussion of section 4.5.2 it is reasonable to assume that the sticking channel is dominant. Doyle et al. established the absence of the direct channel by varying the surface temperature. By measuring the decay rate of the sample when temperature and wall collision rate are known, $s(E)$ may be extracted. The results are shown in fig. 16. The sticking probability does not fall off but rather increases at decreasing temperature. A plausible explanation for this phenomenon may be a resonance phenomenon as in the theory of Goldman [75]. Hijmans et al. [70] used a realistic adsorption potential and claim that resonant enhancement may only be explained if substrate effects dominate the adsorption. Carraro and Cole [93] arrive at the same conclusion and show that the agreement with the low-temperature experimental data may be improved by including corrections to the DWBA approximation used by Hijmans et al. These corrections typically lead to an increase of the sticking probability by a factor of 2. Other theoretical arguments that may lead to large sticking are presented by Martin et al. [94], but it is not clear whether this theory is applicable here.

Looking at the future there are various interesting continuations of the ongoing research of atom surface scattering. The most systematic approach is to aim for energy- and angular-resolved scattering experiments. In this way uncertainties associated with thermal averaging may be avoided and the narrow quasi-elastic peak may be resolved. Such an effort is a very demanding task. Other ways to fingerprint direct-inelastic scattering is to vary atom energy and surface-temperature independently. Also the effect of ^{3}He coverages on the scattering deserves to be further investigated. To measure the low-temperature sticking limit on liquid helium, bulk liquid

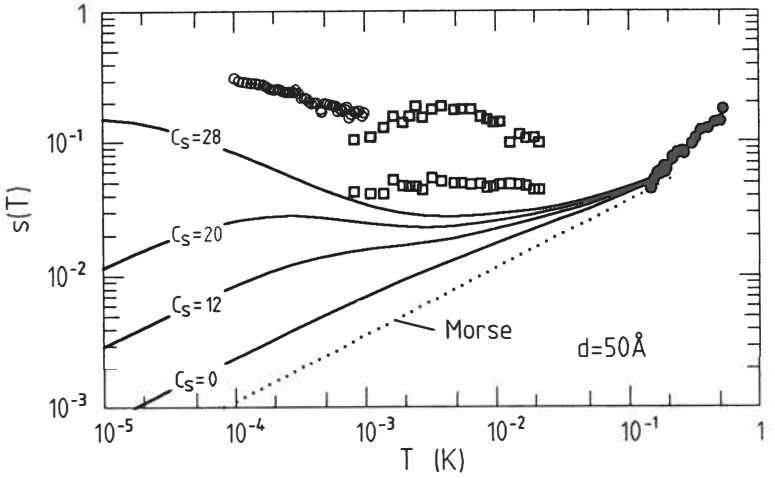

Fig. 16. Sticking probability versus atom energy. The open circles and squares are the results of Doyle et al. [92]. The solid dots are the results of Berkhout et al. [85]. For a global comparison the theoretical model results of Hijmans et al. [70] (for normal incidence) are given.

should be used. By substrate variation, the importance of substrate effects at low temperatures may be demonstrated.

The future of helium covered mirrors is hard to assess. To manipulate H-atom beams they may proof valuable. A logical continuation of the mirror experiments could be diffraction experiments on a ruled grating covered with liquid helium. Helium covered zone-plates could be used (in reflection) to velocity select and focus H-beams. This may prove an interesting alternative to time-of-flight scattering experiments.

Acknowledgements

Many discussions with colleagues have been valuable in relation to this work. In particular I would like to thank Jaap Berkhout, Tom Hijmans, Yuri Kagan, Gora Shlyapnikov and the organizers of the Les Houches summerschool for providing the context in which this paper could be written. The work on atomic hydrogen at the University of Amsterdam is part of the research program of the Stichting voor Fundamenteel Onderzoek der Materie (FOM), which is financially supported by the Nederlandse Organisatie voor wetenschappelijk onderzoek (NWO). Also support from the NWO-PIONIER program is gratefully acknowledged.

References

[1] T.J. Greytak and D. Kleppner, Lectures on spin-polarized hydrogen, in: New trends in atomic physics, Vol. II, eds. G. Grynberg and R. Stora, Elsevier, Amsterdam (1984) pp. 1125–1230.

[2] I.F. Silvera and J.T.M. Walraven, Spin-polarized Atomic Hydrogen, Prog. Low Temp. Phys., ed. D.F. Brewer, Elsevier Sci. Publ. **X** (1986) 139–370.

[3] W.N. Hardy, M. Morrow, R. Jochemsen and A.J. Berlinsky, Magnetic resonance of atomic hydrogen at low temperatures, Physica **B 109&110** (1982) 1964–1977 (LT-16).

[4] W.N. Hardy, M.D. Hürlimann and R.W. Cline, Application of atomic hydrogen at low temperature: The recirculating cryogenic hydrogen maser, Jpn. J. Appl. Phys. **26** (1987) 2065–2072 (LT-18).

[5] J.H. Freed, Spin waves in spin-polarized H↓, Ann. Phys. (Paris) **10** (1985) 901–921 (Kastler Symposium).

[6] D.M. Lee, Spin waves in spin-polarized hydrogen, Jpn. J. Appl. Phys. **26** (1987) 1841–1848 (LT-18).

[7] E.R. Cohen and B.N. Taylor, The 1986 adjustment of the fundamental physical constants, Rev. Mod. Phys. **59** (1987) 1121–1148.

[8] G. Breit and I.I. Rabi, Measurement of nuclear spin, Phys. Rev. (1931) 2082–2083.

[9] W. Kolos and L. Wolniewicz, Potential energy curve for the X-$^1\Sigma_g^+$, b-$^3\Sigma_u^+$ and C $^1\Pi_u$ states of the hydrogen molecule, J. Chem. Phys. **43** (1965) 2429–2441.

[10] W. Kolos and L. Wolniewicz, Variational calculation of the long-range interaction between two ground-state hydrogen atoms, Chem. Phys. Lett. **24** (1974) 457–460.

[11] W. Kolos and L. Wolniewicz, Improved potential energy curve and vibrational energies for the electronic ground state of the hydrogen molecule, J. Mol. Spectrosc. **54** (1975) 303–311.

[12] W. Kolos, K. Szalewicz and H.J. Monkhortst, New Born–Oppenheimer potential energy curve and vibrational energies for the electronic ground state of the hydrogen molecule, J. Chem. Phys. **84** (1986) 3278–3283.

[13] I.F. Silvera, The solid molecular hydrogens in the condensed phase: Fundamentals and static properties, Rev. Mod. Phys. **52** (1980) 393–452.

[14] M.D. Miller, Theory of boson mixtures, Phys. Rev. **B 18** (1978) 4730–4738.

[15] M.D. Miller, The ground state of binary boson mixtures, Ann. Phys. (NY) **127** (1980) 367–412.

[16] R.A. Guyer and M.D. Miller, Interaction of atomic hydrogen with the surface of liquid ^{4}He, Phys. Rev. Lett. **42** (1979) 1754–1757.

[17] M.L. Ristig, S. Fantoni and K.E. Kürten, Ground state properties of boson mixtures, Z. Phys. **B 51** (1983) 1–9.

[18] K.E. Kürten and M.L. Ristig, Atomic and molecular hydrogen isotopes in liquid helium, Phys. Rev. **B 31** (1985) 1346–1351.

[19] E. Tjukanov, P.C. Souers and W.N. Hardy, Zero-field magnetic resonance studies of atomic tritium, in: Spin-polarized quantum systems, ed. S. Stringari (World Scientific Publ., Singapore, 1989) 240–243.

[20] D.O. Edwards and W.F. Saam, The free surface of liquid helium, Prog. Low Temp. Phys., ed. D.F. Brewer **VIIA** (1978) 283–369.

[21] D.O. Edwards, ^{4}He surfaces, Physica **B 109&110** (1982) 1531–1541.

[22] A.F.G. Wyatt and H.J.Lauter, eds., Excitations in two-dimensional and three-dimensional quantum liquids, **NATO ASI B 257** (Plenum Press, New York, 1991).

[23] J. Wilks, The properties of liquid and solid helium (Clarendon Press, Oxford, 1967).
[24] G. Baym and C. Pethick, Low temperature properties of dilute solutions of ^{3}He in superfluid ^{4}He, in: The physics of liquid and solid helium, part II, eds. K.H. Bennemann and J.B. Ketterson, John Wiley, New York (1978) 123–175.
[25] M.W. Reynolds, M.E. Hayden and W.N. Hardy, J. Low Temp. Phys. **84** (1991) 87–108.
[26] J. Ruvalds, Excitations in ^{3}He-^{4}He mixtures, in: Quantum liquids, eds. J. Ruvalds and T. Regge, North-Holand Publ., Amsterdam (1978) 263–291.
[27] D.R. Tilley and J. Tilley, Superfluidity and superconductivity (Adam Hilger, Bristol, 1986).
[28] A.L. Fetter, Vortices and ions in liquid helium, in: The physics of liquid and solid helium, part I, eds. K.H. Bennemann and J.B. Ketterson, John Wiley, New York (1976) 207–305.
[29] P.V.E. McClintock and R.M. Bowley, Vortex creation in superfluid helium-4, in: Excitations in two-dimensional and three-dimensional quantum liquids, eds. A.F.G. Wyatt and H.J.Lauter, **NATO ASI B 257**, Plenum Press, New York (1991) 567–578.
[30] S. Stringari and J. Treiner, Surface properties of liquid ^{3}He and ^{4}He: A density-functional approach, Phys. Rev. **B 36** (1987) 8369–8375.
[31] W.C. Stwalley, Simple long-range model and scaling relations for the binding of isotopic hydrogen atoms to isotopic helium surfaces, Chem. Phys. Lett. **88** (1982) 404–408.
[32] I.B. Mantz and D.O. Edwards, Binding of spin-polarized hydrogen to the free surface of liquid helium, Phys. Rev. **B 20** (1979) 4518–4526.
[33] C. De Simone and B. Maraviglia, Atomic H on liquid He surface: Interaction and bound states, Chem. Phys. Lett. **60** (1979) 289–291.
[34] E. Krotscheck, M. Saarela and J.L. Epstein, Impurity states in liquid helium films, in: Spin-polarized quantum systems, ed. S. Stringari, World Scientific Publ., Singapore (1989) 116–120.
[35] R.P. Feynman, Atomic theory of the two-fluid model of liquid helium, Phys. Rev. **94** (1954) 262–277.
[36] J. Lekner, Theory of surface states of ^{3}He atoms in liquid ^{4}He, Philos. Mag. **22** (1970) 669–673.
[37] D.O. Edwards and P.P. Fatouros, Theory of atomic scattering at the free surface of liquid ^{4}He, Phys. Rev. **B 17** (1978) 2147–2159.
[38] A. Messiah, Quantum mechanics (North-Holland, Amsterdam, 1970).
[39] I.F. Silvera and V.V. Goldman, Atomic hydrogen in contact with a helium surface: Bose condensation, adsorption isotherms, and stability, Phys. Rev. Lett. **45** (1980) 915–918.
[40] D.O. Edwards and I.B. Mantz, The adsorption of atomic hydrogen on the surface of 4-He, J. Phys. (Paris) **C 7-41** (1980) 257–265.
[41] J.M. Kosterlitz and D.J. Thouless, J. Phys. **C 6** (1973) 1181–1203.
[42] J.M. Kosterlitz and D.J. Thouless, Two-dimensional physics, Progr. Low Temp.Phys. ed. D.F. Brewer, North-Holland, Amsterdam **VII-B** (1978) 372–433.
[43] V.N. Popov, Functional integrals in quantum field theory and statistical physics, D. Reidel Publ. Dordrecht (1983).
[44] Yu. Kagan, B.V. Svistunov and G.V. Shlyapnikov, Influence on inelastic processes of the phase transition in a weakly collisional two-dimensional Bose gas, Sov. Phys. JETP **66** (1987) 314–323.

[45] B.V. Svistunov, T.W. Hijmans, G.V. Shlyapnikov and J.T.M. Walraven, Resonant light absorption and the problem of observing the Kosterlitz–Thouless transition in spin-polarized hydrogen adsorbed on a liquid helium surface., Phys. Rev. **B 43** (1991) 13, 412
[46] L.D. Landau and E.M. Lifshitz, Statistical physics (part 2), (Pergamon Press, Oxford, 1980).
[47] D.J. Friend and R.D. Etters, A hard-sphere Bose-gas model calculation of low-density atomic hydrogen gas properties, J. Low Temp. Phys. **39** (1980) 409–415.
[48] B.J. Verhaar, J.P.H.W. van den Eijnde, M.A.J. Voermans and M.M.J. Schaffrath, Scattering length and effective range in two dimensions; application to adsorbed hydrogen atoms, J. Phys. **A 17** (1984) 595–598.
[49] Yu. Kagan, G.V. Shlyapnikov, I.A. Vartanyantz and N.A. Glukhov, Quasi-two-dimensional spin-polarized atomic hydrogen, JETP Lett. **35** (1982) 477–481.
[50] B.J. Verhaar, private communication (1985).
[51] M. Schick, Two-dimensional system of hard-core bosons, Phys. Rev. **A 3** (1971) 1067–1073.
[52] L.W. Bruch, Two-dimensional many-body problem I. The low-density hard-disk Bose gas, Physica **A 93** (1978) 95–113.
[53] Yu. Kagan, N.A. Glukhov, B.V. Svistunov and G.V. Shlyapnikov, Collective phenomena in adsorbed H↓ phase of limiting density, Phys. Lett. **A 135** (1989) 219–222.
[54] W.F. Saam, Quantum theory of superfluidity and its onset in Bose films, Phys. Rev. **B 23** (1981) 1485 1488.
[55] S.I. Shevchenko, Fluctuation correlation and superfluidity in a two-dimensional film of atomic hydrogen, Sov. J. Low Temp. Phys. **8** (1982) 221–227.
[56] D.S. Fisher and P.C. Hohenberg, Dilute Bose gas in two dimensions, Phys. Rev. **B 37** (1988) 4936–4943.
[57] M.D. Miller and L.H. Nosanow, Liquid-to-gas phase transitions in two-dimensional quantum systems at zero temperature, J. Low Temp. Phys. **32** (1978) 145–157.
[58] L.J. Lantto and R.M. Nieminen, Calculated properties of two-dimensional spin-polarized atomic hydrogen, J. Phys. (Paris) **C 7-41** (1980) 49–50 (Aussois).
[59] J.P.H.W van den Eijnde, C.J. Reuver and B.J. Verhaar, Improvements in the description of the surface spin relaxation of atomic hydrogen, Phys. Rev. B **28** (1983) 6309–6314.
[60] R.D. Etters, R.L. Danilowicz and R.W. Palmer, Low-density properties of gaseous, spin-aligned atomic hydrogen, J. Low Temp. Phys. **33** (1978) 305–311.
[61] L.J. Lantto and R.M. Nieminen, Properties of condensed spin-aligned atomic hydrogen from variational calculations, J. Low Temp. Phys. **37** (1979) 1–12.
[62] V.V. Goldman and I.F. Silvera, Exchange interactions and adsorption isotherms of spin-polarized atomic hydrogen on helium, Physica **B 107** (1981) 515–516 (LT-16).
[63] K. Huang, Statistical mechanics, (Wiley, New York, 1963).
[64] P.C. Hohenberg, Existence of long-range order in one and two dimensions, Phys. Rev. **158** (1967) 383–386.
[65] N.N. Bogoliubov, On the theory of superfluidity, J. Phys. (Moscow) **11** (1947) 23–32.
[66] K.R. Atkins, Ripplons and the critical velocity of the helium film, Physica **23** (1957) 1143-1144.
[67] M. Iino, M. Suzuki and A.J. Ikushima, Surface tension of liquid ^{4}He. Surface energy of the Bose–Einstein condensate, J. Low Temp. Phys. **61** (1985) 155–169.
[68] M.W. Cole, Width of the surface layer of liquid ^{4}He, Phys. Rev. **A 1** (1970) 1838–

1840.
[69] T.W. Hijmans, private communication (1991).
[70] T.W. Hijmans, J.T.M. Walraven and G.V. Shlyapnikov, On the influence of the substrate on the low temperature limit of the sticking probability of hydrogen atoms on He films, Phys. Rev. **B 45** (1992) 2561–2564.
[71] D.S. Zimmerman and A.J. Berlinsky, The sticking probability for hydrogen atoms on the surface of liquid ^{4}He, Can. J. Phys. **61** (1983) 508–513.
[72] Yu. Kagan and G.V. Shlyapnikov, On the possibility of attaining the Bose-condensation region in spin-polarized atomic hydrogen at ultra-low temperatures, Phys. Lett. **A 95** (1983) 309–312.
[73] Yu. Kagan, N.A. Glukhov, B.V. Svistunov and G.V. Shlyapnikov, Kapitza resistance in H↓ gas at limiting density, preprint (1990).
[74] Yu. Kagan, G.V. Shlyapnikov and N.A. Glukhov, Kapitza jump in a gas of spin-polarized atomic hydrogen, JETP Lett. **40** (1984) 1072–1076.
[75] V.V. Goldman, Kapitza conductance between gaseous atomic hydrogen and liquid helium, Phys. Rev. Lett. **56** (1986) 612–615.
[76] J. Böheim, W. Brenig and J. Stutzki, On the low-energy limit of reflection and sticking coefficients in atom surface scattering. 2 Long range forces, Z. Phys. **B 48** (1982) 43–49.
[77] E. Tiesinga, H.T.C. Stoof and B.J. Verhaar, Reflection of hydrogen atoms from the surface of superfluid helium, Phys. Rev. **B 41** (1990) 8886–8890.
[78] B. Castaing and M. Papoular, Kapitza resistance at the H↓/liquid He interface, J. Phys. (Paris) Lett. **44** (1983) L537–L540.
[79] B.W. Statt, Thermal accommodation of atomic hydrogen with a liquid ^{4}He surface, Phys. Rev. **B 32** (1985) 7160–7164.
[80] T.W. Hijmans and G.V. Shlyapnikov, Small angle inelastic scattering of hydrogen atoms from a liquid He surface, Phys. Lett. **142** (1989) 45 48.
[81] R. Jochemsen, M. Morrow, A.J. Berlinsky and W.N. Hardy, Interaction of hydrogen atoms with helium films: sticking probabilities for H on ^{3}He and ^{4}He, and binding energy of H on ^{3}He, Phys. Rev. Lett. **47** (1981) 852–855.
[82] M. Morrow and W.N. Hardy, The magnetic resonance lineshape for atomic hydrogen confined by liquid helium walls, Can. J. Phys. **61** (1983) 956–963.
[83] J.J Berkhout, E.J. Wolters, R. van Roijen and J.T.M. Walraven, Vanishing sticking probabilities and enhanced capillary flow of spin-polarized hydrogen, Phys. Rev. Lett. **57** (1986) 2387–2390.
[84] J.P. Laheurte, J.C. Noiray and J.P. Romagnan, Interface between two thin ^{3}He–^{4}He liquid mixtures films, in: Excitations in two-dimensional and three-dimensional quantum liquids, eds. A.F.G. Wyatt and H.J. Lauter, **NATO ASI B 257** Plenum Press, New York (1991) 429–437.
[85] J.J Berkhout, O.J. Luiten, I.D. Setija, T.W. Hijmans, T. Mizusaki and J.T.M. Walraven, Quantum reflection: focussing of hydrogen atoms with a concave mirror, Phys. Rev. Lett. **63** (1989) 1689–1692.
[86] J.J Berkhout, O.H. Höpfner, E.J. Wolters and J.T.M. Walraven, Sensitive bolometric detection of atomic hydrogen fluxes, Jpn. J. Appl. Phys. **26** (1987) 231–232 LT-18.
[87] K. Salonen, I.F. Silvera, J.T.M. Walraven and G.H. van Yperen, Ballistic heat pulses in spin-polarized atomic hydrogen to $T = 200$ mK, Phys. Rev. **B 25** (1982) 6002–6005.
[88] K. Salonen, S. Jaakkola, M. Karhunen, E. Tjukanov and T. Tommila, Thermal

accommodation of atomic hydrogen on saturated ^{4}He film, Proceedings LT-17, eds. U. Eckern, A. Schmid, W. Weber, H. Wühl, Elsevier Science Publ., Amsterdam (1984) 543.

[89] D.A. Bell, H.F. Hess, G.P. Kochanski, S. Buchman, L. Pollack, Y.M. Xiao, D. Kleppner and T.J. Greytak, Relaxation and recombination in spin-polarized atomic hydrogen, Phys. Rev. **B 34** (1986) 7670–7697.

[90] J. Helffrich, M. Maley, M. Krusius and J.C. Wheatley, Measurement of thermal accommodation of spin-polarized hydrogen on a saturated ^{4}He film at 0.18–0.4 K, Phys. Rev. **B 34** (1986) 6550–6553.

[91] J.J. Berkhout and J.T.M. Walraven, to be published.

[92] J.M. Doyle, J.C. Sandberg, I.A. Yu, C.L. Cesar, D. Kleppner and T.J. Greytak, Hydrogen in the submillikelvin regime: Sticking probability on superfluid ^{4}He, Phys. Rev. Lett. **67** (1991) 603–606.

[93] C. Carraro and M.W. Cole, **45** (1992) 12930–12935.

[94] Th. Martin, R. Bruinsma and P.M. Platzman, Critical-like behavior in quantum adsorption, Phys. Rev. **B 39** (1989) 12411–12413.